sample preparation, and matrix-assisted laser desorption ionization tandem time-of-flight mass spectrometry analysis. *J. Biol. Chem.* **286,** 41669–41679
21. Yanagisawa, K., and Matsuzaki, K. (2002) Cholesterol-dependent aggregation of amyloid β-protein. *Ann. N.Y. Acad. Sci.* **977,** 384–386
22. Yuyama, K., and Yanagisawa, K. (2010) Sphingomyelin accumulation provides a favorable milieu for GM1 ganglioside-induced assembly of amyloid β-protein. *Neurosci. Lett.* **481,** 168–172
23. Trajkovic, K., Hsu, C., Chiantia, S., Rajendran, L., Wenzel, D., Wieland, F., Schwille, P., Brügger, B., and Simons, M. (2008) Ceramide triggers budding of exosome vesicles into multivesicular endosomes. *Science* **319,** 1244–1247
24. Takata, K., Hirata-Fukae, C., Becker, A. G., Chishiro, S., Gray, A. J., Nishitomi, K., Franz, A. H., Sakaguchi, G., Kato A., Mattson, M. P., Laferla, F. M., Aisen, P. S., Kitamura, Y., and Matsuoka, Y. (2007) Deglycosylated anti-amyloid β antibodies reduce microglial phagocytosis and cytokine production while retaining the capacity to induce amyloid β sequestration. *Eur. J. Neurosci.* **26,** 2458–2468
25. Gulbins, E., and Kolesnick, R. (2003) Raft ceramide in molecular medicine. *Oncogene* **22,** 7070–7077
26. Simons, K., and Ikonen, E. (1997) Functional rafts in cell membranes. *Nature* **387,** 569–572
27. de Gassart, A., Geminard, C., Fevrier, B., Raposo, G., and Vidal, M. (2003) Lipid raft-associated protein sorting in exosomes. *Blood* **102,** 4336–4344
28. Keilani, S., Lun, Y., Stevens, A. C., Williams, H. N., Sjoberg, E. R., Khanna, R., Valenzano, K. J., Checler, F., Buxbaum, J. D., Yanagisawa, K., Lockhart, D. J., Wustman, B. A., and Gandy, S. (2012) Lysosomal dysfunction in a mouse model of Sandhoff disease leads to accumulation of ganglioside-bound amyloid-β peptide. *J. Neurosci.* **32,** 5223–5236
29. Xu, Y. H., Barnes, S., Sun, Y., and Grabowski, G. A. (2010) Multi-system disorders of glycosphingolipid and ganglioside metabolism. *J. Lipid Res.* **51,** 1643–1675
30. Bolmont, T., Haiss, F., Eicke, D., Radde, R., Mathis, C. A., Klunk, W. E., Kohsaka, S., Jucker, M., and Calhoun, M. E. (2008) Dynamics of the microglial/amyloid interaction indicate a role in plaque maintenance. *J. Neurosci.* **28,** 4283–4292
31. Matsuzaki, K., Kato, K., and Yanagisawa, K. (2010) Aβ polymerization through interaction with membrane gangliosides. *Biochim. Biophys. Acta* **1801,** 868–877
32. Hong, S., Ostaszewski, B. L., Yang, T., O'Malley, T. T., Jin, M., Yanagisawa, K., Li, S., Bartels, T., and Selkoe, D. J. (2014) Soluble Aβ oligomers are rapidly sequestered from brain ISF *in vivo* and bind GM1 ganglioside on cellular membranes. *Neuron* **82,** 308–319
33. Fevrier, B., Vilette, D., Archer, F., Loew, D., Faigle, W., Vidal, M., Laude, H., and Raposo, G. (2004) Cells release prions in association with exosomes. *Proc. Natl. Acad. Sci. U.S.A.* **101,** 9683–9688
34. Emmanouilidou, E., Melachroinou, K., Roumeliotis, T., Garbis, S. D., Ntzouni, M., Margaritis, L. H., Stefanis, L., and Vekrellis, K. (2010) Cell-produced α-synuclein is secreted in a calcium-dependent manner by exosomes and impacts neuronal survival. *J. Neurosci.* **30,** 6838–6851
35. Martinez, Z., Zhu, M., Han, S., and Fink, A. L. (2007) GM1 specifically interacts with α-synuclein and inhibits fibrillation. *Biochemistry* **46,** 1868–1877
36. Sanghera, N., Correia, B. E., Correia, J. R., Ludwig, C., Agarwal, S., Nakamura, H. K., Kuwata, K., Samain, E., Gill, A. C., Bonev, B. B., and Pinheiro, T. J. (2011) Deciphering the molecular details for the binding of the prion protein to main ganglioside GM1 of neuronal membranes. *Chem. Biol.* **18,** 1422–1431
37. Fitzner, D., Schnaars, M., van Rossum, D., Krishnamoorthy, G., Dibaj, P., Bakhti, M., Regen, T., Hanisch, U. K., and Simons, M. (2011) Selective transfer of exosomes from oligodendrocytes to microglia by macropinocytosis. *J. Cell Sci.* **124,** 447–458
38. Frühbeis, C., Fröhlich, D., Kuo, W. P., Amphornrat, J., Thilemann, S., Saab, A. S., Kirchhoff, F., Möbius, W., Goebbels, S., Nave, K. A., Schneider, A., Simons, M., Klugmann, M., Trotter, J., and Krämer-Albers, E. M. (2013) Neurotransmitter-triggered transfer of exosomes mediates oligodendrocyte-neuron communication. *PLoS Biol.* **11,** e1001604
39. Tamboli, I. Y., Barth, E., Christian, L., Siepmann, M., Kumar, S., Singh, S., Tolksdorf, K., Heneka, M. T., Lütjohann, D., Wunderlich, P., and Walter, J. (2010) Statins promote the degradation of extracellular amyloid β-peptide by microglia via stimulation of exosome-associated insulin-degrading enzyme (IDE) secretion. *J. Biol. Chem.* **285,** 37405–37414
40. Katsuda, T., Tsuchiya, R., Kosaka, N., Yoshioka, Y., Takagaki, K., Oki, K., Takeshita, F., Sakai, Y., Kuroda, M., and Ochiya, T. (2013) Human adipose tissue-derived mesenchymal stem cells secrete functional neprilysin-bound exosomes. *Sci. Rep.* **3,** 1197
41. Alvarez-Erviti, L., Seow, Y., Yin, H., Betts, C., Lakhal, S., and Wood, M. J. (2011) Delivery of siRNA to the mouse brain by systemic injection of targeted exosomes. *Nat. Biotechnol.* **29,** 341–345
42. Zhuang, X., Xiang, X., Grizzle, W., Sun, D., Zhang, S., Axtell, R. C., Ju, S., Mu, J., Zhang, L., Steinman, L., Miller, D., and Zhang, H. G. (2011) Treatment of brain inflammatory diseases by delivering exosome encapsulated anti-inflammatory drugs from the nasal region to the brain. *Mol. Ther.* **19,** 1769–1779

THE JOURNAL OF BIOLOGICAL CHEMISTRY VOL. 290, NO. 7, pp. 3894–3909, February 13, 2015

Protein-tyrosine Phosphatase Shp2 Positively Regulates Macrophage Oxidative Burst*

Received for publication, September 23, 2014, and in revised form, December 23, 2014 Published, JBC Papers in Press, December 23, 2014, DOI 10.1074/jbc.M114.614057

Xing Jun Li[‡§1], Charles B Goodwin[§¶], Sarah C. Nabinger[¶], Briana M. Richine[§¶], Zhenyun Yang[‖], Helmut Hanenberg[‡§¶], Hiroshi Ohnishi[‡‡], Takashi Matozaki[§§], Gen-Sheng Feng[¶¶], and Rebecca J. Chan[‡§¶2]**

*From the [‡]Department of Pediatrics, the [§]Herman B Wells Center for Pediatric Research, and the [¶]Department of Medical & Molecular Genetics, Indiana University School of Medicine, Indianapolis, Indiana 46202, [‖]West Coast University, Los Angeles, California 91606, the **Department of Otorhinolaryngology and Head/Neck Surgery, Heinrich Heine University, 40225 Düsseldorf, Germany, the [‡‡]Gunma University Graduate School of Health Sciences, Maebashi, Gunma 371-8514, Japan, the [§§]Kobe University Graduate School of Medicine, Chuo-Ku, Kobe 650-0017, Japan, and the [¶¶]Department of Pathology, University of California, San Diego, La Jolla, California 92093*

Background: Innate immune cell oxidative burst is needed to combat pathogens.
Results: Loss of Shp2 phosphatase reduces, whereas increased Shp2 phosphatase function enhances, ROS production.
Conclusion: The Shp2 phosphatase domain is specifically required for optimal oxidative burst in macrophages.
Significance: Humans bearing aberrancies of Shp2 phosphatase or of Shp2-containing signaling pathways may be prone to impaired or excessive ROS production.

Macrophages are vital to innate immunity and express pattern recognition receptors and integrins for the rapid detection of invading pathogens. Stimulation of Dectin-1 and complement receptor 3 (CR3) activates Erk- and Akt-dependent production of reactive oxygen species (ROS). Shp2, a protein-tyrosine phosphatase encoded by *Ptpn11*, promotes activation of Ras-Erk and PI3K-Akt and is crucial for hematopoietic cell function; however, no studies have examined Shp2 function in particulate-stimulated ROS production. Maximal Dectin-1-stimulated ROS production corresponded kinetically to maximal Shp2 and Erk phosphorylation. Bone marrow-derived macrophages (BMMs) from mice with a conditionally deleted allele of *Ptpn11* ($Shp2^{flox/flox}$;Mx1Cre+) produced significantly lower ROS levels compared with control BMMs. Although YFP-tagged phosphatase dead Shp2-C463A was strongly recruited to the early phagosome, its expression inhibited Dectin-1- and CR3-stimulated phospho-Erk and ROS levels, placing Shp2 phosphatase function and Erk activation upstream of ROS production. Further, BMMs expressing gain of function Shp2-D61Y or Shp2-E76K and peritoneal exudate macrophages from Shp2D61Y/+;Mx1Cre+ mice produced significantly elevated levels of Dectin-1- and CR3-stimulated ROS, which was reduced by pharmacologic inhibition of Erk. SIRPα (signal regulatory protein α) is a myeloid inhibitory immunoreceptor that requires tyrosine phosphorylation to exert its inhibitory effect. YFP-Shp2C463A-expressing cells have elevated phospho-SIRPα levels and an increased Shp2-SIRPα interaction compared with YFP-WT Shp2-expressing cells. Collectively, these findings indicate that Shp2 phosphatase function positively regulates Dectin-1- and CR3-stimulated ROS production in macrophages by dephosphorylating and thus mitigating the inhibitory function of SIRPα and by promoting Erk activation.

Macrophages are phagocytic cells that function as the body's global first line defense against invading pathogens. Upon interaction with pathogen-producing stimuli, macrophages internalize large particulate microorganisms and generate microbicidal reactive oxygen species (ROS)[3] produced by activated NADPH oxidase (1). NADPH oxidase is composed of membrane-integrated $gp91^{phox}$ and $p22^{phox}$, as well as the four cytosolic components $p47^{phox}$, $p67^{phox}$, $p40^{phox}$, and Rac2 (2, 3). Individuals with chronic granulomatous disease have inherited germ line mutations within variable components of the NADPH oxidase complex and suffer from recurrent, life-threatening bacterial and fungal infections, highlighting the imperative nature of competent ROS production by the innate immunity (4, 5).

Shp2, a protein-tyrosine phosphatase encoded by the *PTPN11* gene, promotes activation of Ras-Erk signaling and plays an essential role in hematopoietic cell development (6, 7). Genetic disruption of murine *Ptpn11* within hematopoietic lineages leads to rapid loss of blood cell production of all lineages (8, 9). In humans, gain of function *PTPN11* mutations are commonly found in children with Noonan syndrome and juvenile myelomonocytic leukemia (10, 11). Although no *PTPN11* mutations have been found to be associated with clinical immune deficiency, Shp2 is a critical signaling component of leptin receptor-dependent protection against the parasitic

* This work was supported, in whole or in part, by National Institutes of Health Grant RO1 CA134777 (to R. J. C.). This work was also supported by funds from the Showalter Research Trust (to X. J. L.), the Riley Children's Foundation, and the Indiana University-Purdue University Indianapolis Office of the Vice Chancellor for Research.

[1] To whom correspondence may be addressed: Dept. of Pediatrics, Indiana University School of Medicine, Indianapolis, IN 46202. Tel.: 317-274-4719; Fax: 317-278-8679; E-mail: xl9@iu.edu.

[2] To whom correspondence may be addressed: Dept. of Pediatrics, Indiana University School of Medicine, Indianapolis, IN 46202. Tel.: 317-274-4719; Fax: 317-278-8679; E-mail: rchan@iu.edu.

[3] The abbreviations used are: ROS, reactive oxygen species; BMM, bone marrow-derived macrophage; GOF, gain of function; PEM, peritoneal exudate macrophage; SOZ, serum opsonized zymosan; IMDM, Iscove's modified Dulbecco's medium; DPI, diphenyleneiodonium chloride; IP, immunoprecipitation.

pathogen *Entamoeba histolytica* (12), and children bearing germ line loss of function *LEPR* mutations are susceptible to respiratory infections (13). Further, previous studies found that Shp2 regulates the phosphorylation of transcription factors HoxA10 and ICSBP, leading to transcriptional repression of the NADPH oxidase components gp91^{phox} and p67^{phox} and preventing myeloid terminal differentiation (14, 15); however, no studies have examined the function of Shp2 phosphatase in ROS production in terminally differentiated macrophages or neutrophils, which may reveal a novel role for Shp2 in innate immunity and ROS production.

Macrophages are capable of detecting and responding to pathogen-derived molecules such as fungal glucans and lipopolysaccharides, because they express cell surface pattern recognition receptors such as C-type lectins. Dectin-1 is a C-type lectin expressed on macrophages that responds to β-glucan-containing particles derived from fungal cell walls and stimulates Src- and Syk-dependent signaling (16). Dectin-1 stimulation results in activation of the Ras-Erk pathway, production of microbicidal ROS, and induction of expression of the inflammatory cytokines TNFα and IL6. In humans, loss of function mutations in *DECTIN-1* confer a state of increased susceptibility to mucocutaneous *Candida albicans* and invasive aspergillosis (17, 18).

Based on the known high expression of Shp2 in macrophages and its well defined role as a positive regulator of the Ras-Erk pathway, we hypothesized that Shp2 promotes normal innate immunity by positively up-regulating particulate-stimulated NADPH oxidase activation and abrupt production of ROS, known as oxidative burst. To address this hypothesis, we examined the correlation of Shp2 activation to peak ROS production in zymosan-stimulated peritoneal exudate macrophages (PEMs) and examined the putative placement of Shp2 in the Dectin-1-stimulated pathway employing genetic studies and pharmacologic studies using the Syk inhibitor R406 and the Erk inhibitor SCH772984. Genetic disruption of *Ptpn11* resulted in reduced macrophage ROS production in response to both zymosan (Dectin-1 stimulation) and serum opsonized zymosan (SOZ, complement receptor 3 stimulation), indicating a positive function of Shp2 in oxidative burst. Structure-function studies using various Shp2 loss of function and gain of function constructs indicated that the phosphatase function of Shp2 is specifically required for positive regulation of particulate-stimulated oxidative burst. Mechanistic studies demonstrated that Shp2 exerts its positive effect on ROS generation by dephosphorylating the myeloid inhibitory immunoreceptor, SIRPα (signal regulatory protein α), and by promoting Erk activation.

EXPERIMENTAL PROCEDURES

Reagents—Chemicals were purchased from Sigma-Aldrich unless otherwise stated. PBS, pH 7.2, penicillin/streptomycin, neomycin, IMDM, and DMEM were from Invitrogen; FCS was from HyClone Laboratory (Logan, UT). The ECL detection kit came from Pierce. Rabbit polyclonal antibody against p40^{phox} and mouse monoclonal antibody T-Syk were from Upstate Biotechnology (Lake Placid, NY), rabbit polyclonal antibody against p47^{phox} was from Santa Cruz Biotechnology (Santa Cruz, CA), and monoclonal antibody against p67^{phox} was from BD Biosciences. Rabbit polyclonal and mouse monoclonal antibodies against Shp2 were from Santa Cruz Biotechnology (catalog no. SC-280) and BD Biosciences (catalog no. 610621), respectively. Anti-SIRPα polyclonal antibody was from Abcam (catalog no. 53721), and mouse dectin-1/CLEC7A antibody (clone 218838) was from R&D Systems, Inc. (Minneapolis, MN). Anti-phospho-SIRPα was generated as previously described (19). Anti-gp91^{phox} mAb 54.1 and anti-p22^{phox} mAb NS2 were kindly provided by A. J. Jesaitis (Montana State University) (20). All the other antibodies, including anti-phospho-antibodies, were obtained from Cell Signaling Technology (Beverly, MA) unless otherwise stated. Zymosan A from *Saccharomyces cerevisiae* was from Sigma (Z-4250). The FITC-labeled zymosan particles were from Invitrogen. Phycoerythrin-Mac-1 and allophycocyanin-F4/80 were from BD Pharmingen.

Animal Husbandry—Mice bearing a conditional gain of function (GOF) *Ptpn11* allele (*LSL-Shp2*$^{D61Y/+}$) or a conditional floxed *Ptpn11* allele (*Shp2*$^{flox/flox}$) have been described (9, 21, 22) and were crossed with mice bearing the Mx1Cre transgene to generate experimental (Shp2D61Y;Mx1Cre+ or Shp2$^{f/f}$;MxCre+) and negative control (Shp2D61Y;Mx1Cre− or Shp2$^{f/f}$;MxCre−) animals. All animals received three intraperitoneal injections with 300 μg of poly(I·C) (GE Healthcare) to induce *Ptpn11* recombination. All mice were maintained under specific pathogen-free conditions at the Indiana University Laboratory Animal Research Center (Indianapolis, IN), and this study was approved by the Institutional Animal Care and Use Committee of the Indiana University School of Medicine.

Plasmid Construction—The cDNAs encoding WT Shp2 or Shp2-R32K and Shp2-C463A mutants were cloned into EcoRI and KpnI sites of pEYFP-N1 (Clontech) to generate YFP-tagged Shp2 constructs, and the constructs were confirmed by sequencing. The YFP-tagged Shp2 cDNAs were then ligated into pMSCV (Clontech) for use in generation of retroviral supernatants. Preparation and characterization of the pMIEG3-WT Shp2, Shp2-D61Y, and Shp2-E76K was described previously (23).

Retroviral Transduction of Bone Marrow and Macrophage Differentiation—Retroviral transduction of murine bone marrow low density mononuclear cells (C57Bl/6 background) with MSCV-WT Shp2-YFP, Shp2-R32K-YFP, or Shp2-C463A-YFP or with MIEG3-WT Shp2, Shp2-D61Y, or Shp2-E76K was performed as described (23, 24). Transduced cells were sorted by fluorescence-activated cell sorting (FACSCalibur; BD Biosciences) prior to macrophage differentiation, as described (23). Activity, immunostaining, and live images were analyzed 6–7 days after macrophage differentiation.

PEM Preparation—Eight weeks after poly(I·C) treatment, Shp2D61Y;Mx1Cre+ and negative control Shp2D61Y;Mx1Cre− animals were injected with 1 ml of 3% thioglycollate to induce peritoneal inflammation. 72 h later, peritoneal cells were harvested by lavage with PBS, and macrophages were isolated by culturing cells at 1×10^6 cells/ml in IMDM with 20% heat-inactivated serum and 2% penicillin-streptomycin in a tissue culture dish for 2 h and then removing nonadherent cells (25). After overnight incubation in IMDM with 20% heat-inactivated serum and 2% penicillin-streptomycin, PEMs were used to perform functional and biochemical analyses.

Preparation of Particulate Stimuli—Zymosan and SOZ A particles (Sigma; Z-4250) were prepared as previously described (26–28). A synchronized phagocytosis assay was used for zymosan- or SOZ-induced NADPH oxidase activity assays (29, 30). Briefly, macrophages in 200 μl of PBSG (PBS plus 0.9 mM $CaCl_2$, 0.5 mM $MgCl_2$, and 20 mM dextrose) were incubated on ice for 5 min in 50 μM luminol and 20 units/ml HRP, and then 25 μl of cold zymosan or SOZ (final concentration, 400 μg/ml) were added. Cells and particles were spun at 1200 rpm for 5 min at 4 °C and then immediately placed at 37 °C in the luminometer.

ROS Detected by Chemiluminescence in Intact Cells—ROS production during synchronized phagocytosis of SOZ or zymosan stimulation was measured in the presence of 20 μM luminol with 20 units/ml HRP (24, 30, 31). An Lmax microplate luminometer (Molecular Devices, Sunnyvale, CA) was used to record luminescence as previously described (24, 26). For some experiments, macrophages were preincubated at 37 °C with Syk inhibitor, R406, NADPH oxidase inhibitor, diphenyleneiodonium chloride (DPI), or Erk inhibitor for 30 min.

Phagocytosis Assays—Synchronized phagocytosis was performed as previously described (24). Briefly, 2×10^6 macrophages were washed with PBS and resuspended in 3 ml of PBSG, added to 6-well plate, and kept on ice for 5 min, followed by adding 300 μl of cold SOZ or zymosan (4.4 μg/μl in PBSG) for a final concentration of 400 μg/ml. Plates were immediately centrifuged at 1200 rpm for 5 min at 4 °C and then transferred to 37 °C for indicated time. For biochemical studies, cells were washed in 3× PBS, and 60 μl of lysis buffer was added to each well. For the phagocytic assays, the macrophages were plated at 0.5×10^6 cells/well in 12-well plates in macrophage differentiation medium incubated at 37 °C for 24 h. After washing, FITC-labeled zymosan particles (100 μg/ml) (Molecular Probes, Invitrogen) were added to the cells, and cells were incubated at 37 °C for indicated time. The cells were then put on ice and washed thoroughly to remove unbound particles with PBS. The macrophages were detached and analyzed by flow cytometry immediately.

Western Blots—Macrophages were lysed in lysis buffer containing 50 mM Hepes (pH 7.4), 150 mM NaCl, 10% glycerol, 1% Triton X-100, 1.5 mM $MgCl_2$, 1 mM EGTA,100 mM NaF, 10 mM sodium pryophosphate, 1 mM PMSF, 1× protease inhibitor mixture set I (Calbiochem), 1 mM Na_3VO_4, and 0.1 mM $ZnCl_2$ (32, 33). 10 μg of protein lysate was subjected to SDS-PAGE and immunoblotting using ECL detection (24, 26). YFP expression was also analyzed by flow cytometry (FACSCalibur; BD Biosciences) (24, 26).

Immunoprecipitation (IP)—100 μg of cell lysates were adjusted to a total volume of 1 ml in IP incubation buffer (50 mM Hepes, pH 7.4, 1% Triton X-100, 150 mM NaCl, 5 mM EDTA, 0.1% BSA, 50 mM NaF, 1 mM PMSF, 1× protease inhibitor mixture set I (Calbiochem), 1 mM Na_3VO_4, and 0.1 mM $ZnCl_2$). 2 μg of anti-Shp2 polyclonal antibody (SC-280; Santa Cruz Biotechnology) was added to the cell lysates and incubated at 4 °C for 1 h, followed by addition of 25 μl of protein A/G Plus-agarose (Santa Cruz Biotechnology) and incubated for 2–3 h at 4 °C. The beads was washed three times in buffer (50 mM Hepes, pH 7.4, 1% Triton X-100, 120 mM NaCl, 5 mM EDTA, 50 mM NaF, 1 mM PMSF, 1× protease inhibitor mixture set I (Calbiochem), 1 mM Na_3VO_4, and 0.1 mM $ZnCl_2$), resuspended in 25 μl of 2× SDS-PAGE loading buffer, and boiled for 5 min, and supernatant was subjected to SDS-PAGE and immunoblotting with anti-phospho-SIRPα or anti-Shp2.

Immunofluorescence Microscopy—Immunostaining for Shp2 was performed after synchronized phagocytosis. Briefly, 1×10^6 PEMs or BMMs in 2 ml of PBSG were added to coverslip-bottomed dishes (MatTek Cultureware, Ashland, MA) and incubated for 5 min on ice prior to adding 300 μl of zymosan or SOZ (final concentration, 400 μg/ml). The cells and particles were spun down at 1200 rpm for 5 min at 4 °C and then incubated at 37 °C for 10 min for PEMs or 30 min for BMMs. Phagocytosis was terminated by placing the cells on ice, which were then washed with cold PBS, fixed with 4% paraformaldehyde for 10 min at room temperature, permeabilized with 0.1% Triton X-100 in PBS, blocked with 10% goat serum plus 2% BSA in PBS, and immunostained with anti-Shp2 followed by Alexa Fluor 568 goat anti-rabbit IgG. For co-staining, cells were immunostained with anti-SIRPα polyclonal Ab (catalog no. 53721; Abcam) and anti-Shp2 mAb (catalog no. 610621; BD Biosciences) followed by Alexa Fluor 568 goat anti-rabbit IgG and Alexa Fluor 488 goat anti-mouse IgG1. Cells were imaged on a spinning disk (CSU10) confocal system mounted on a Nikon TE-2000U inverted microscope with an Ixon air-cooled EMCCD camera (Andor Technology, South Windsor, CT) and a Nikon Plan Apo 100× 1.4 N.A. objective. Images shown are representative of at least three independent experiments.

Live Cell Imaging by Confocal Videomicroscopy—SOZ-induced phagocytosis in WT mouse BMMs expressing YFP-tagged WT Shp2, Shp2-C463A, or Shp2-R32K was filmed using a spinning disk (CSU10) confocal system mounted on a Nikon TE-2000U inverted microscope with an Ixon air-cooled EMCCD camera (Andor Technology, South Windsor, CT) and a Nikon Plan Apo 100× 1.4 N.A. objective as described previously. All images were analyzed with Metamorph software (Universal Imaging, Downington, PA). Each type of experiment was performed on at least three independent occasions. Live images were collected in a single confocal plane (1 μM) with 514-nm excitation and 0.3 s of exposure with a time lapse of 10 s.

Statistical Analysis—Groups were compared using unpaired, two-tailed, Student's *t* test.

RESULTS

Shp2 Functions Downstream of Syk in Dectin-1 Signaling—Previous work has demonstrated that Dectin-1 stimulation with β-glucan-containing particles leads to Ras-Erk pathway activation and ROS production in a Syk-dependent manner (16). Given that the protein-tyrosine phosphatase Shp2 positively regulates Ras-Erk pathway signaling and is known to be crucial for normal hematopoietic cell development and function (6, 7), we hypothesized that Shp2 functions in the Dectin-1 signaling pathway to promote particulate-stimulated ROS production in macrophages. To address this hypothesis, we used PEMs to examine the kinetics of Shp2 phosphorylation at tyrosine 580 (indicating that Shp2 is in its open, active conformation) (34) in response to zymosan and correlated Shp2 phosphorylation with peak ROS production and activation of the known Dectin-1-responsive signaling molecules, Syk, Erk, and Akt. Zymosan exposure induced maximal ROS production at

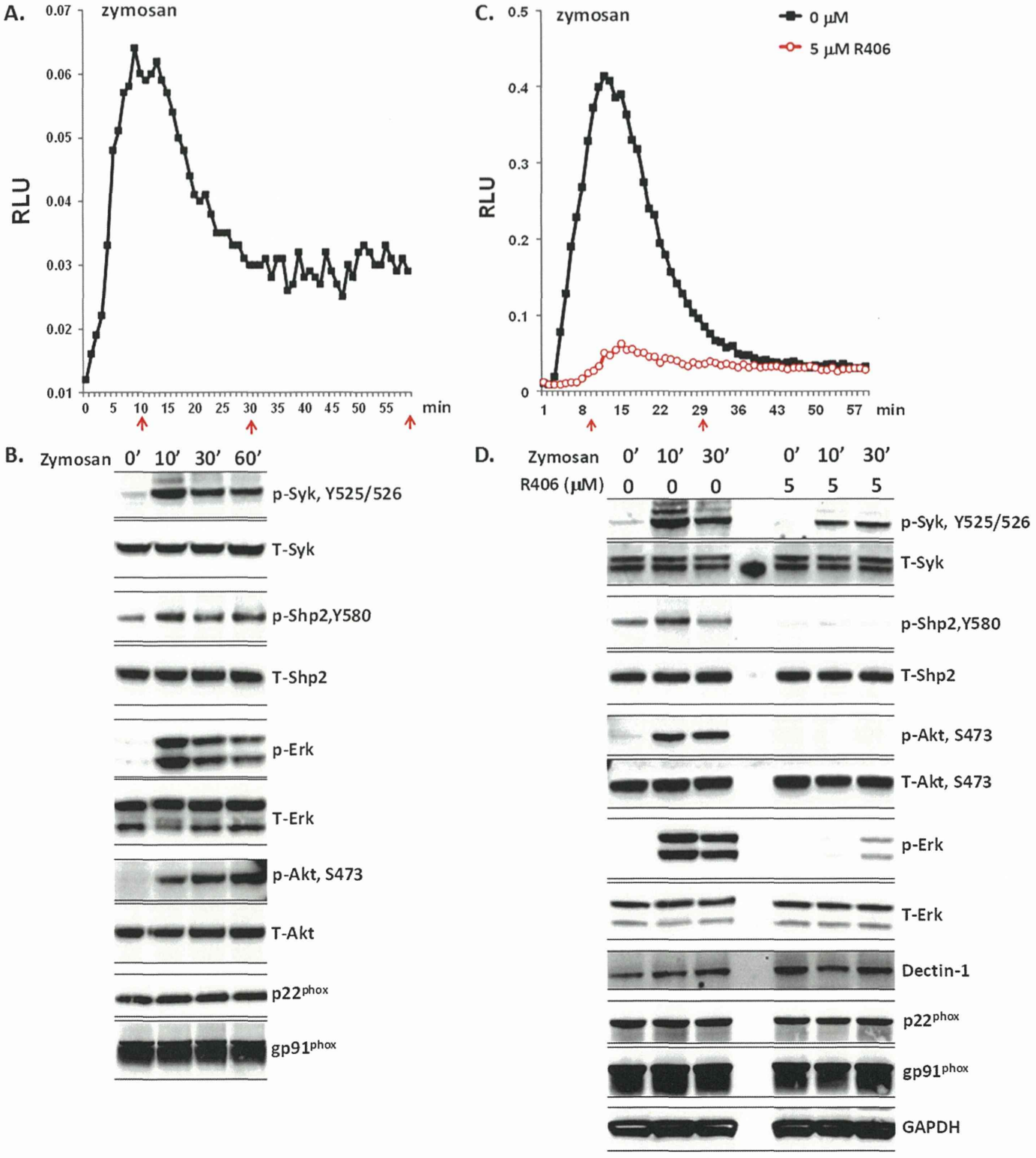

FIGURE 1. **Zymosan-induced ROS production and the activation of Dectin-1-stimulated signaling molecules in WT mouse PEMs.** *A*, ROS production in 0.01 × 10^6 PEMs upon zymosan (400 μg/ml) stimulation. *B*, immunoblot demonstrating phosphorylation of Syk, Shp2, Erk, and Akt at different time points during zymosan-triggered activation in mouse PEMs. *C*, ROS production in 0.05 × 10^6 PEMs upon zymosan (400 μg/ml) stimulation in the absence or presence of the Syk inhibitor R406 (5 μm). *D*, immunoblot demonstrating phosphorylation of Syk, Shp2, Erk, and Akt at different time points during zymosan-triggered activation in mouse PEMs in the absence or presence of Syk inhibitor R406 (5 μm). 10 μg of cell lysate was used in immunoblotting. Assays were performed in triplicate. *RLU*, relative light units.

10 min poststimulation, and this time point corresponded to maximal activation of Syk, Shp2, and Erk (Fig. 1, *A* and *B*). As expected, Akt was also activated by zymosan stimulation; however, peak Akt activation was at 1 h poststimulation and after the peak ROS production, suggesting that Akt serves to support sustained ROS production rather than promoting immediate

and maximal ROS production. Upon treatment with the Syk inhibitor, R406, ROS production was strongly suppressed, which correlated kinetically with reduced Syk, Shp2, Erk, and Akt activation (Fig. 1, *C* and *D*). Importantly, R406 treatment did not suppress expression of $p22^{phox}$ and $gp91^{phox}$ (Fig. 1*D*), suggesting that reduced ROS is not due to altered expression of NADPH oxidase components but is instead due to reduced NADPH oxidase function.

Genetic Disruption of Shp2 Results in Reduced Zymosan- and SOZ-stimulated ROS Production—We next used a mouse model bearing a conditionally floxed allele of *Ptpn11* ($Shp2^{f/f}$;Mx1Cre+) (9). $Shp2^{f/f}$;Mx1Cre+ and negative control $Shp2^{f/f}$;Mx1Cre− mice were treated with 300 μg of poly(I·C) every other day for three doses. 4–6 weeks following poly(I·C) treatment, animals were euthanized followed by isolation of bone marrow low density mononuclear cells, which were cultured in M-CSF to generate BMMs. Based on Mac1 and F4/80 staining, cultured BMMs from the $Shp2^{f/f}$;Mx1Cre+ and $Shp2^{f/f}$;Mx1Cre− mice demonstrated a similar level of terminal differentiation (Fig. 2*A*). However, following stimulation with zymosan (Dectin-1 stimulation) or with SOZ (complement receptor 3 stimulation), the $Shp2^{f/f}$;Mx1Cre+ BMMs demonstrated a reduced oxidative burst compared with the $Shp2^{f/f}$;Mx1Cre− BMMs (Fig. 2, *B–D*). Because Shp2 had previously been found to regulate FcγR-induced phagocytosis in macrophages (35), we next examined whether the reduced ROS production was due to a global reduction in phagocytosis; however, the phagocytic index was similar for the $Shp2^{flox/flox}$;Mx1Cre+ and $Shp2^{flox/flox}$;Mx1Cre− BMMs (Fig. 2*E*). Moreover, we found that expression of various components of the NADPH oxidase complex ($p22^{phox}$, $gp91^{phox}$, $p40^{phox}$, $p47^{phox}$, and $p67^{phox}$) were expressed at similar levels in the $Shp2^{f/f}$;Mx1Cre+ and $Shp2^{f/f}$;Mx1Cre− BMMs (Fig. 2*F*), indicating that the reduced ROS seen in the $Shp2^{flox/flox}$;Mx1Cre+ BMMs is not due to reduced expression of *phox* proteins.

When examining Dectin-1 signaling, both total Shp2 and phospho-Shp2 levels were reduced in the $Shp2^{f/f}$;Mx1Cre+ BMMs, and as anticipated Erk activation was reduced in a correlative fashion (Fig. 2*G*). Reduced Shp2 expression did not have an effect on overall phospho-Akt levels, suggesting that the Shp2-regulated Erk activation is more relevant to abrupt and maximal ROS production. Consistent with the pharmacologic data using R406, reduced Shp2 expression and activation did not cause reduced activation of Syk. Collectively, these functional and biochemical studies suggest that Shp2 functions downstream of Syk in the Dectin-1-stimulated signaling pathway and positively up-regulates Dectin-1-stimulated ROS levels.

Shp2 Is Recruited to the Phagosome and Requires Tyrosine Phosphatase Function to Promote ROS Production—Given the positive role of Shp2 on zymosan- and SOZ-stimulated ROS production, we next imaged SOZ-stimulated BMMs to determine whether Shp2 is recruited to the phagosome membrane, the location of the NADPH oxidase complex. Consistent with the positive functional findings, we found that Shp2 strongly co-localizes with F-actin on the phagosomal cup and early phagosomes (Fig. 3*A*).

To define the biochemical role of Shp2 in ROS production, we generated YFP-tagged Shp2 constructs bearing mutation of the N-SH2 (R32K) or phosphatase (C463A) domains (Fig. 3*B*). These constructs were retrovirally introduced into murine bone marrow low density mononuclear cells followed by sorting to enrich for YFP+ cells and generation of BMMs. Sorted, differentiated macrophages expressed similar levels of each of the Shp2 constructs based on YFP expression (Fig. 3*C*) and immunoblot analysis (Fig. 3*D*), expressed similar levels of the NADPH oxidase components, $p67^{phox}$, $p22^{phox}$, and $gp91^{phox}$ (Fig. 3*D*), and differentiated similarly based on Mac1 and F4/80 expression (Fig. 3*E*). When subjected to zymosan or SOZ stimulation, mutation of either the N-SH2 domain or the phosphatase domain resulted in reduced ROS production (Fig. 3*F*). Given the functional effect of the N-SH2 domain and phosphatase dead mutants, we next compared the subcellular phagosomal membrane localization of WT Shp2 to the point mutants using time lapse confocal videomicroscopy. The N-SH2 domain mutant was not recruited to the phagosome; however, the phosphatase dead mutant was strongly recruited to the phagosome, even more intensely than WT Shp2 (Fig. 3*G*). These findings suggest that the phosphatase function of Shp2 specifically is needed for the positive regulation of NADPH oxidase.

GOF Shp2 Mutants Enhance Zymosan- and SOZ-stimulated ROS Production—Based on the finding that expression of phosphatase dead Shp2-C463A resulted in reduced ROS production, we reasoned that macrophages expressing juvenile myelomonocytic leukemia-associated GOF Shp2 mutants (10, 23), characterized to have increased phosphatase activity (10, 36), would produce elevated zymosan- and SOZ-stimulated ROS levels. To examine this hypothesis, we retrovirally introduced WT Shp2, Shp2-D61Y, or Shp2-E76K into murine bone marrow low density mononuclear cells followed by *in vitro* differentiation to BMMs. We demonstrated increased total Shp2 expression (compared with vector-transduced cells; Fig. 4*A*); however, the NADPH oxidase protein components were similar in all cells (Fig. 4*A*). As anticipated, BMMs retrovirally expressing GOF Shp2-D61Y or GOF Shp2-E76K produced significantly elevated levels of ROS in response to zymosan and SOZ compared with BMMs retrovirally expressing WT Shp2 (Fig. 4, *B* and *C*). Additionally, Shp2-D61Y was strongly recruited to the SOZ-stimulated phagosomal cup and early phagosome, similar to that seen with WT Shp2 (Fig. 4*D*).

To utilize a more physiologic model, we examined ROS production using PEMs from Shp2D61Y;Mx1Cre+ mice, in which Shp2D61Y is under the endogenous control of the *Ptpn11* promoter (21). PEMs collected from the Shp2D61Y;Mx1Cre− and Shp2D61Y;Mx1Cre+ mice demonstrated a similar level of terminal differentiation based on F4/80 and Mac1 staining (Fig. 5*A*) and expressed similar levels of the NADPH oxidase components, $p40^{phox}$, $p22^{phox}$, and $gp91^{phox}$ (Fig. 5*E*). Consistent with the retrovirally transduced cells, PEMs from Shp2D61Y;Mx1Cre+ mice produced substantially higher levels of zymosan- and SOZ-stimulated ROS compared with PEMs from Shp2D61Y;Mx1Cre− mice (Fig. 5, *B–D*). Using Shp2D61Y;Mx1Cre+ PEMs, we interrogated the Dectin-1-stimulated signaling pathway to further clarify the contribution of Syk, Shp2, Erk, and Akt activation to the elevated ROS production in response to zymosan. As predicted, we found increased phospho-Shp2 and enhanced Erk activation in the GOF Shp2-ex-

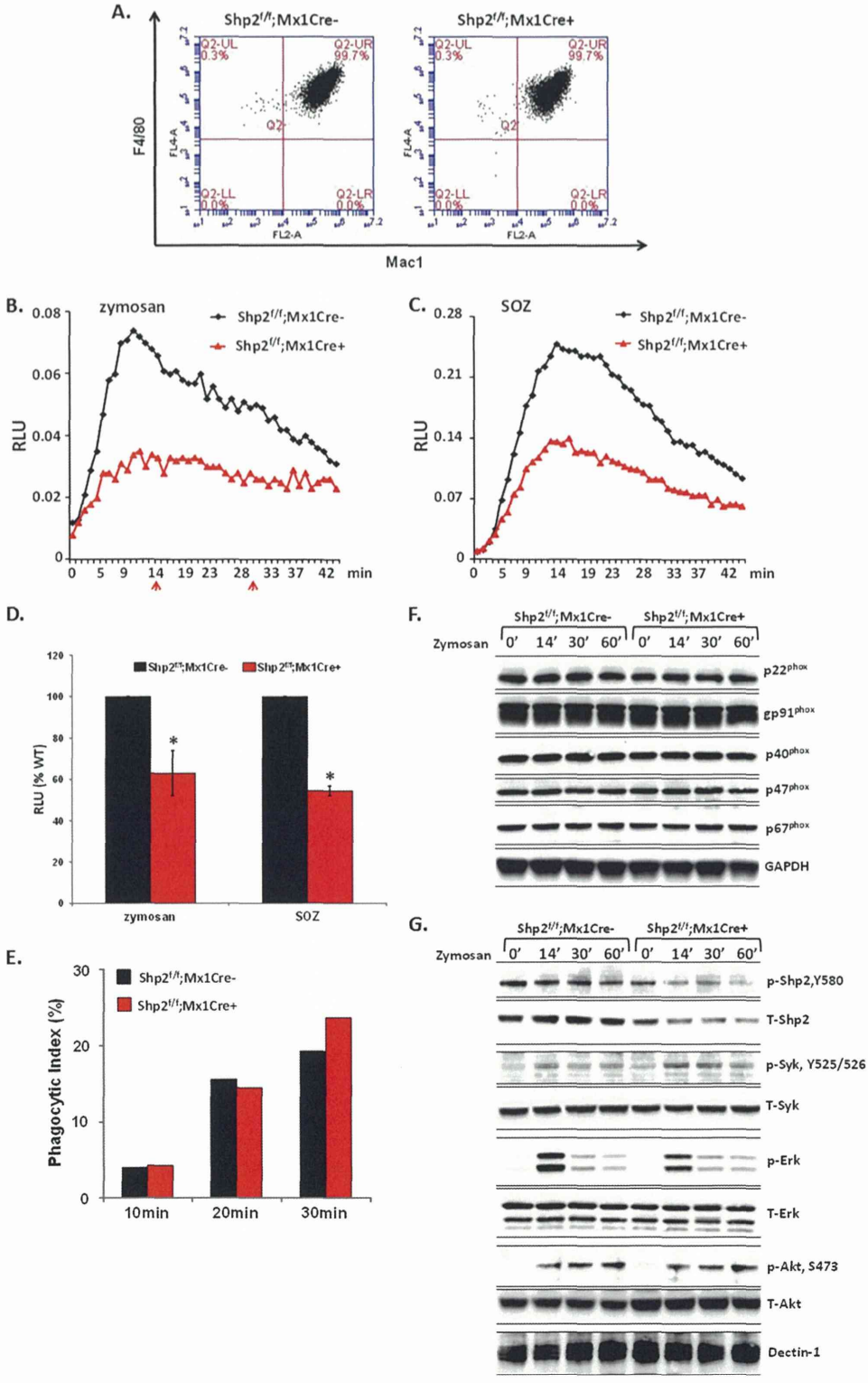

FIGURE 2. **Zymosan- or SOZ-induced ROS production and the activation of Dectin-1-stimulated signaling molecules in Shp2$^{f/f}$;Mx1Cre− and Shp2$^{f/f}$;Mx1Cre+ mouse BMMs.** *A*, flow cytometry demonstrating the expression level of macrophage membrane markers Mac1 and F4/80 in Shp2$^{f/f}$;Mx1Cre− and Shp2$^{f/f}$;Mx1Cre+ BMMs. *B* and *C*, ROS production in 0.05 × 10^6 Shp2$^{f/f}$;Mx1Cre− or Shp2$^{f/f}$;Mx1Cre+ BMMs upon zymosan (*B*) or SOZ (*C*) stimulation. *D*, ROS production compiled from three independent experiments ($n = 3$). *, $p < 0.01$ for Shp2$^{f/f}$;Mx1Cre+ compared with Shp2$^{f/f}$;Mx1Cre− in response to zymosan or SOZ. *E*, phagocytic index. 10,000 cells were analyzed by flow cytometry, and the phagocytic index for each cell type was calculated as described under "Experimental Procedures." *F*, representative immunoblot showing NADPH oxidase *phox* protein expression. *G*, representative immunoblot demonstrating phosphorylation of Shp2, Syk, Erk, and Akt at different time points during zymosan-triggered activation in Shp2$^{f/f}$;Mx1Cre− and Shp2$^{f/f}$;Mx1Cre+ BMMs. *RLU*, relative light units.

pressing cells compared with control cells (Fig. 5*E*). Akt activation was not substantially elevated in the Shp2D61Y-expressing cells, suggesting that Shp2 regulation of Erk activation is more relevant for zymosan-induced maximal ROS production. Interestingly, Erk activation was sustained longer in these cells compared with that observed using WT PEMs (Fig. 1) or the bone

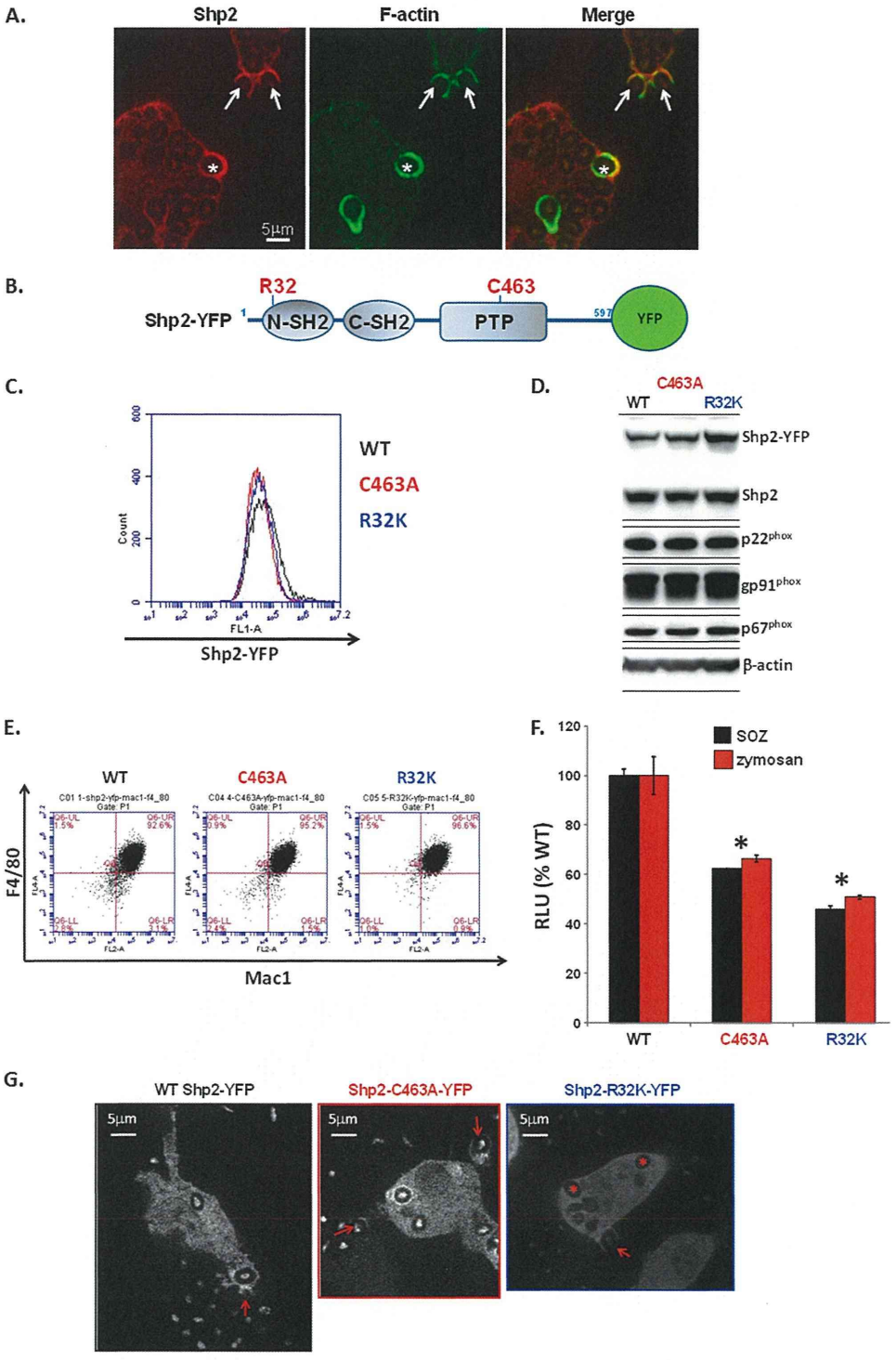

FIGURE 3. **Expression of Shp2 mutants (Shp2-C463A and Shp2-R32K) leads to reduced zymosan- and SOZ-stimulated ROS production.** *A*, localization of endogenous Shp2 upon SOZ stimulation and staining with anti-Shp2 (Santa Cruz, SC-280) and Alexa Fluor 555 goat anti-rabbit IgG in WT BMMS. Alexa Fluor 488 phalloidin was used to stain F-actin, which specifies early phagosomes. *Arrows* and *asterisks* denote Shp2 accumulation on the phagosome cups and early phagosomes, respectively. Representative images from three independent experiments. *B*, structural motifs of YFP-tagged Shp2 constructs. *C*, flow cytometry indicating the expression level of YFP-tagged WT Shp2 (*black*), Shp2-C463A (*red*), or Shp2-R32K (*blue*). *D*, immunoblot demonstrating expression of YFP-tagged Shp2 and endogenous Shp2 in transduced BMMs expressing YFP-tagged WT Shp2, Shp2-C463A, or Shp2-R32K, as well as expression of NADPH oxidase components, $gp91^{phox}$, $p22^{phox}$, and $p67^{phox}$. *E*, flow cytometry demonstrating the expression level of macrophage membrane markers Mac1 and F4/80 in the populations of BMMs expressing YFP-tagged WT Shp2, Shp2-C463A, or Shp2-R32K. *F*, ROS production in BMMs expressing YFP-tagged WT Shp2, Shp2-C463A, or Shp2-R32K compiled from three independent experiments ($n = 3$). *, $p < 0.01$ for Shp2-C463A *versus* WT or Shp2-R32K *versus* WT in response to SOZ or zymosan. *G*, distribution of YFP-tagged WT Shp2, Shp2-C463A, or Shp2-R32K during SOZ-induced phagocytosis in BMMs. *Arrows* indicate the cup of phagosomes, and *asterisks* indicate the internalized phagosomes. *Bars*, 5 μm. *RLU*, relative light units.

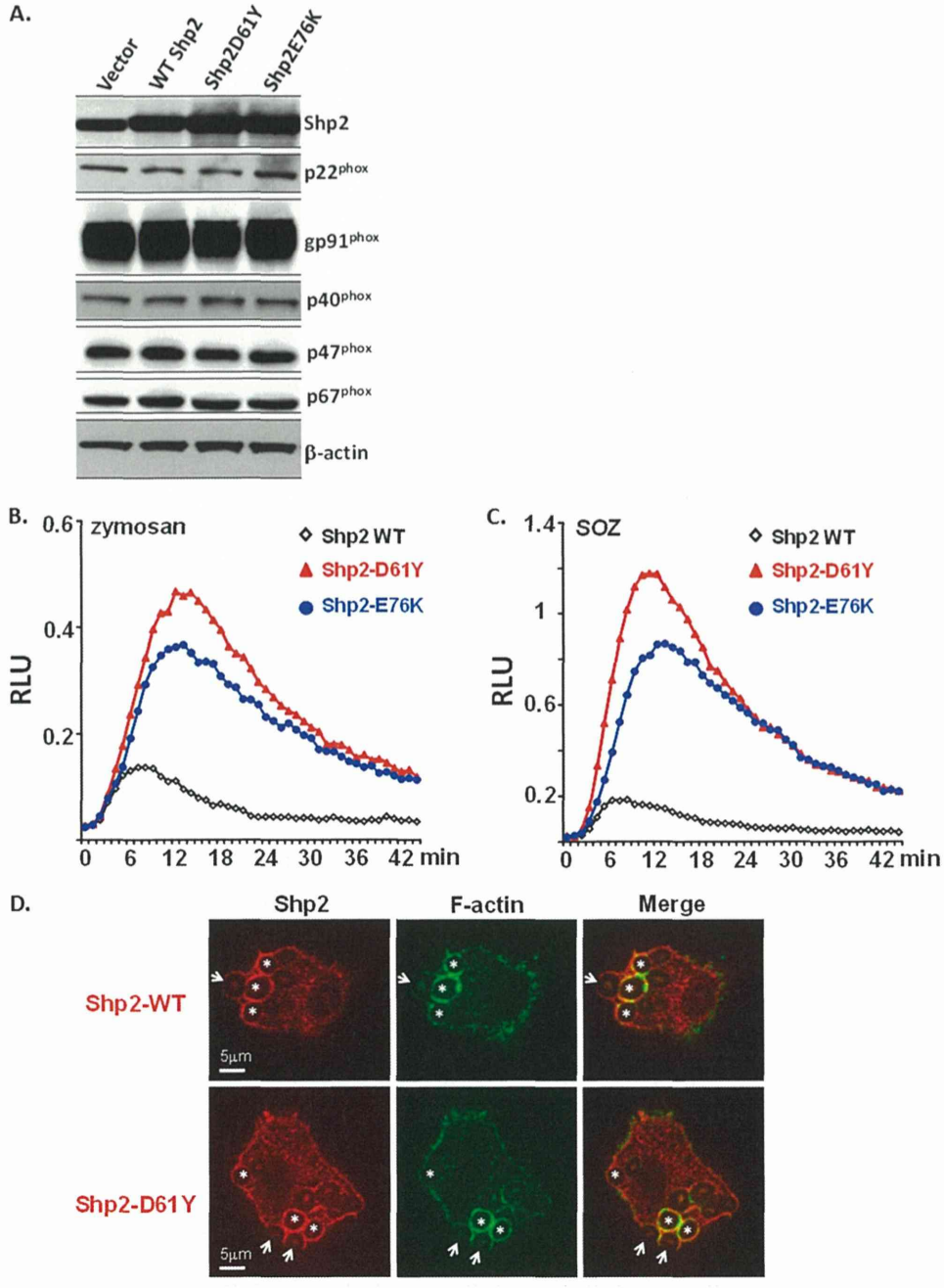

FIGURE 4. **ROS generation in Shp2D61Y- and Shp2E76K-expressing BMMs.** *A*, immunoblot demonstrating Shp2 and *phox* protein expression in WT BMMs retrovirally expressing empty vector (MIEG3), WT Shp2, or GOF mutants Shp2-D61Y and Shp2-E76K. *B* and *C*, ROS production in 0.1×10^6 BMMs expressing WT Shp2 or GOF mutants Shp2-D61Y and Shp2-E76K upon zymosan (*B*) or SOZ (*C*) stimulation. *D*, localization of WT Shp2 and Shp2-D61Y upon SOZ stimulation and immunofluorescent staining with anti-Shp2 (SC-280; Santa Cruz) and Alexa Fluor 555 goat anti-rabbit IgG in WT BMMS. Alexa Fluor 488 phalloidin (Life Technologies) was used to stain F-actin. *Arrows* and *asterisks* denote Shp2 accumulation on the phagosome cups and early phagosomes, respectively. *Bars*, 5 μm. *RLU*, relative light units.

marrow-derived macrophages from $Shp2^{f/f}$;MxCre− mice (Fig. 2). This difference in Erk inactivation kinetics might be due to a strain difference of the Shp2D61Y;Mx1Cre animals, which are on a mixed C57Bl/6-Sv129 background rather than a pure C57Bl/6 background. Notwithstanding, these findings are consistent with the need for Erk to be activated for maximal ROS production; however, they suggest that Erk inactivation is not imperative for the return of ROS to baseline levels. Consistent with previous results using R406 (Fig. 1) and $Shp2^{f/f}$;Mx1Cre+ BMMs (Fig. 2), Syk activation was not altered in the presence of GOF Shp2D61Y (Fig. 5*E*), again suggesting that Shp2 functions downstream of Syk in the Dectin-1 signaling pathway. Together, these findings support a model placing Shp2 downstream of Syk in Dectin-1 signaling and indicate that Shp2 phosphatase function positively regulates NADPH oxidase activity via promoting Erk activation.

Erk Activation Promotes ROS Production in Response to Zymosan Stimulation—Several previous studies have found that ROS *per se* functions as a signaling molecule to promote Erk activation (37). These studies were performed in nonphagocytic cells, and

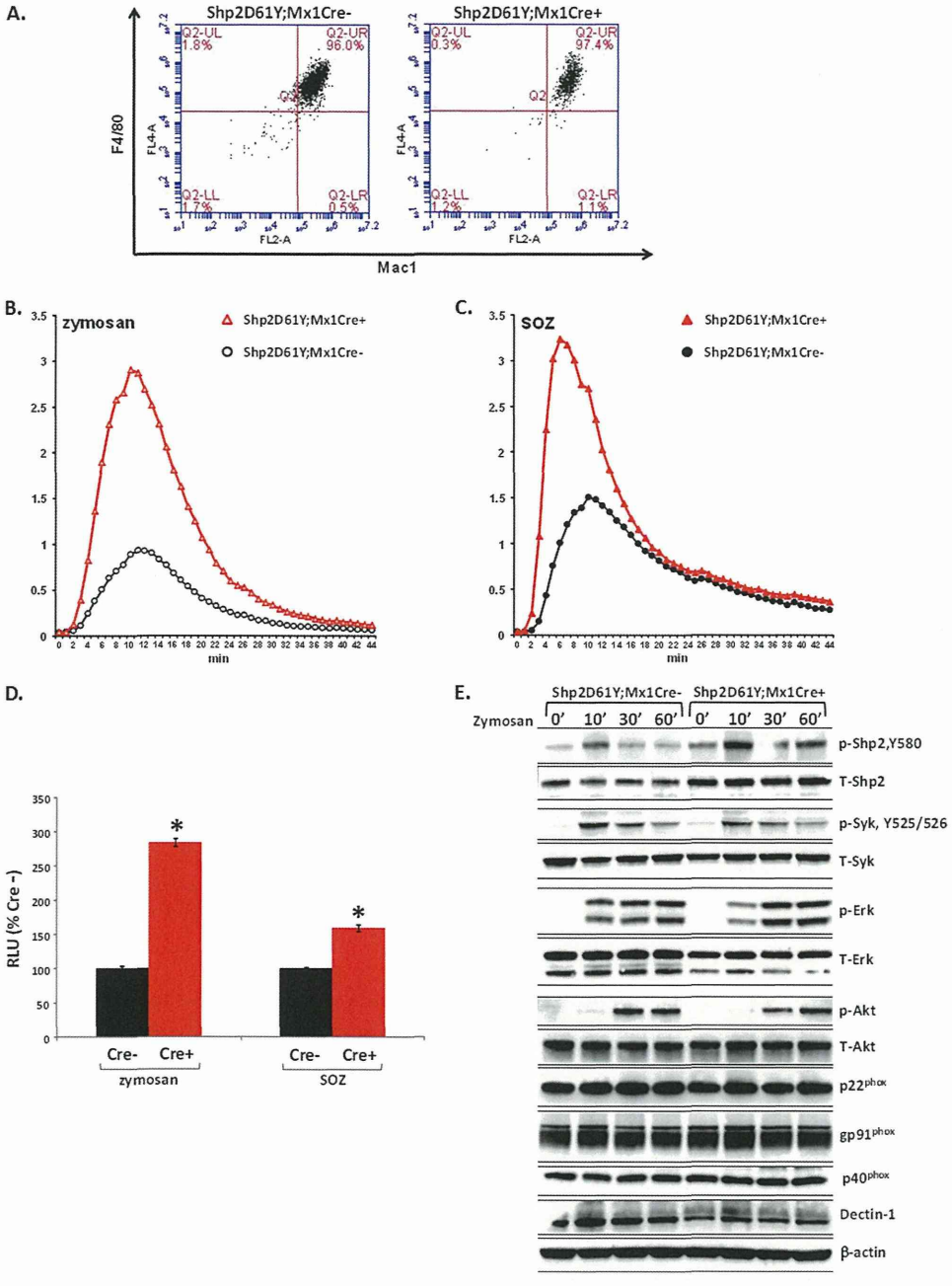

FIGURE 5. **ROS production and the activation of Dectin-1-stimulated signaling molecules in Shp2D61Y;Mx1Cre− and in Shp2D61Y;Mx1Cre+ mouse PEMs upon zymosan or SOZ stimulation.** *A*, flow cytometry demonstrating the expression level of macrophage membrane markers Mac1 and F4/80 in Shp2D61Y;Mx1Cre− and Shp2D61Y;Mx1Cre+ PEMs. *B* and *C*, ROS production in Shp2D61Y;Mx1Cre− and Shp2D61Y;Mx1Cre+ PEMs upon zymosan (*B*) and SOZ (*C*) activation. *D*, ROS production compiled from three independent experiments ($n = 3$). *, $p < 0.01$ for Shp2D61Y;Mx1Cre+ *versus* Shp2D61Y;Mx1Cre− in response to zymosan or SOZ. *E*, representative immunoblot demonstrating protein level of phosphorylated and total Shp2, Syk, Erk, and Akt, as well as *phox* proteins at various time points during zymosan-triggered activation in Shp2D61Y;Mx1Cre− and Shp2D61Y;Mx1Cre+ PEMs. *RLU*, relative light units.

typically the cells were cultured in supraphysiologic concentrations of H_2O_2. On the other hand, other studies demonstrate that Erk promotes NADPH oxidase activation and ROS production (38–40). To determine whether Erk activation is upstream or downstream of ROS in zymosan-stimulated macrophages, we first examined zymosan-stimulated Erk activation in the presence of the conventional NADPH oxidase inhibitor, DPI. Although incubation with DPI essentially obliterated zymosan-stimulated ROS, Erk activation was unchanged (Fig. 6, *A–C*). In concordance with these findings, bone marrow-derived macrophages from X-linked chronic granulomatous disease mice ($gp91^{phox-/-}$) (41), which are devoid of ROS production, also demonstrated no change in zymosan-stimulated phospho-Erk levels (data not shown). We next treated cells with the Erk inhibitor SCH772984 and found a significant reduction of ROS that correlated with reduced Erk activation (Fig. 6, *A–C*), suggesting that Erk functions upstream of zymosan-stimulated oxidative burst. To further define the linear arrangement of Shp2, Erk, and ROS production, we examined the effect of Erk inhibition on ROS production in Shp2D61Y-expressing macrophages. Hyperactivated Erk in Shp2D61Y-expressing macrophages was reduced by treatment with

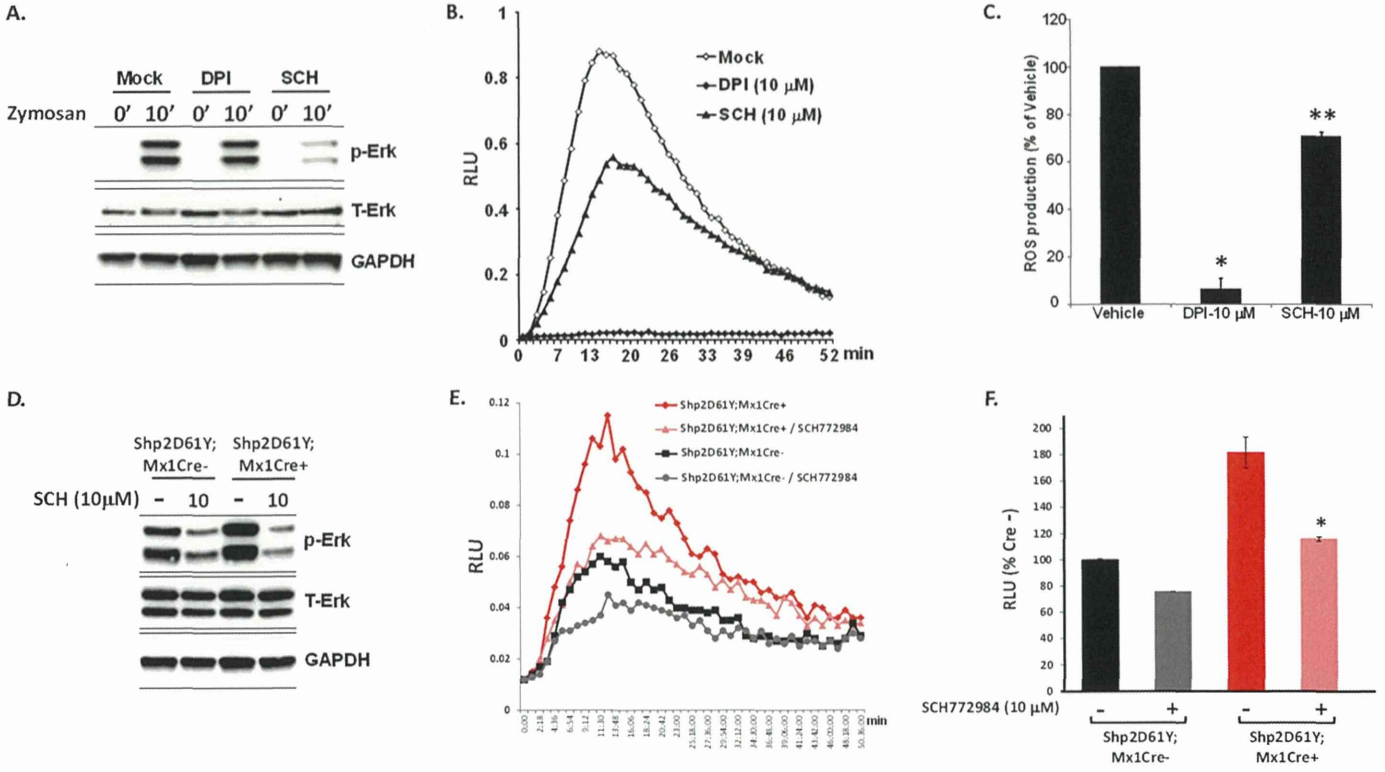

FIGURE 6. **Erk inhibition reduces zymosan-stimulated ROS production.** *A*, representative immunoblot demonstrating p-Erk levels during zymosan-triggered activation in the absence and presence of NADPH oxidase inhibitor DPI or Erk inhibitor SCH1772984. *B*, ROS production in 0.1×10^6 WT PEMs in the presence of DPI or SCH1772984. *C*, ROS production compiled from three independent experiments ($n = 3$). *, $p < 0.0001$ comparing DPI-treated to vehicle-treated; **, $p < 0.01$ for SCH1772984-treated *versus* vehicle-treated. *D*, representative immunoblot demonstrating p-Erk levels in Shp2D61Y;Mx1Cre− and Shp2D61Y;Mx1Cre+ bone marrow-derived macrophages in the absence or presence of Erk inhibitor SCH1772984. *E*, ROS production in 0.03×10^6 Shp2D61Y; Mx1Cre− and Shp2D61Y;Mx1Cre+ bone marrow-derived macrophages in the absence or presence of SCH1772984. *F*, ROS production compiled from three independent experiments ($n = 3$). *, $p < 0.01$ for SCH1772984-treated *versus* vehicle-treated in Shp2D61Y;Mx1Cre+ cells. *RLU*, relative light units; *SCH*, SCH1772984.

SCH772984, similar to that observed with WT Shp2-expressing macrophages (Fig. 6*D*). In a corresponding manner, inhibition with SCH772984 reduced the enhanced ROS levels in the zymosan-stimulated Shp2D61Y-expressing macrophages to near WT levels (Fig. 6, *E* and *F*). These findings support the hypothesis that Erk is downstream of Shp2 and upstream of NADPH oxidase and ROS production in zymosan-stimulated macrophages.

Shp2 and Phospho-SIRPα Co-localize on Phagosomes and Interact Biochemically in Dectin-1-stimulated Cells—Given the positive role of Shp2 phosphatase function in promoting zymosan- and SOZ-stimulated ROS, we investigated putative Shp2 phosphatase substrates that might regulate Erk and NADPH oxidase activation. SIRPα (signal regulatory protein α) is a myeloid inhibitory immunoreceptor highly expressed on macrophages, requires tyrosine phosphorylation to exert its inhibitory effect, and has been shown to be a physiological substrate of Shp2 phosphatase (42, 43). Previous studies indicate that dephosphorylation of SIRPα leads to increased NFκB-stimulated expression of inflammatory cytokines and NADPH oxidase protein components such as $gp91^{phox}$ (19, 44). However, because we see a rapid effect of the various Shp2 mutants on ROS production independent of the time needed for NFκB-stimulated gene expression and protein synthesis, we anticipated that zymosan- or SOZ-stimulated SIRPα dephosphorylation would be correlated with NADPH oxidase activation and ROS production.

To address this hypothesis, we first examined the subcellular localization of SIRPα in zymosan-stimulated PEMs and found that SIRPα is strongly associated with the phagosome membrane at 10 min poststimulation, which correlates kinetically with zymosan-stimulated Shp2 activation and ROS production (data not shown). We next conducted co-localization studies between Shp2 and SIRPα on the phagosome membrane at peak ROS production and found that indeed Shp2 and SIRPα co-localize on phagosome membranes (Fig. 7*A*). However, the actual percentage of phagosomes showing co-localization of Shp2 and SIRPα at peak ROS production was only ~10–15% of phagosomes. Given the relatively low prevalence of Shp2-SIRPα co-localization at the time of peak ROS production, as well as the previous observation that phosphatase dead Shp2-C463A remained more strongly associated with the phagosome membrane compared with WT Shp2 (Fig. 3*G*), we hypothesized dephosphorylation of SIRPα and disruption, rather than maintenance, of the Shp2-SIRPα interaction is needed for maximal activation of NADPH oxidase.

To examine this idea further, we examined zymosan-stimulated phospho-SIRPα levels and correlated phospho-SIRPα with ROS production. As predicted, the phospho-SIRPα level was lowest at the time of maximal ROS production (10 min after zymosan stimulation; Fig. 7*B*) and at the time of maximal Shp2 phosphorylation (Fig. 1*B*). If SIRPα is a substrate of Shp2 in response to phagocytic stimuli, we predicted that cells

expressing phosphatase dead Shp2-C463A would demonstrate elevated phospho-SIRPα levels in response to Dectin-1 stimulation. Accordingly, we found substantially higher levels of phospho-SIRPα at baseline and in response to zymosan stimulation in the Shp2-C462A-expressing BMMs compared with the WT Shp2-expressing cells (Fig. 7*C*). Importantly, the ele-

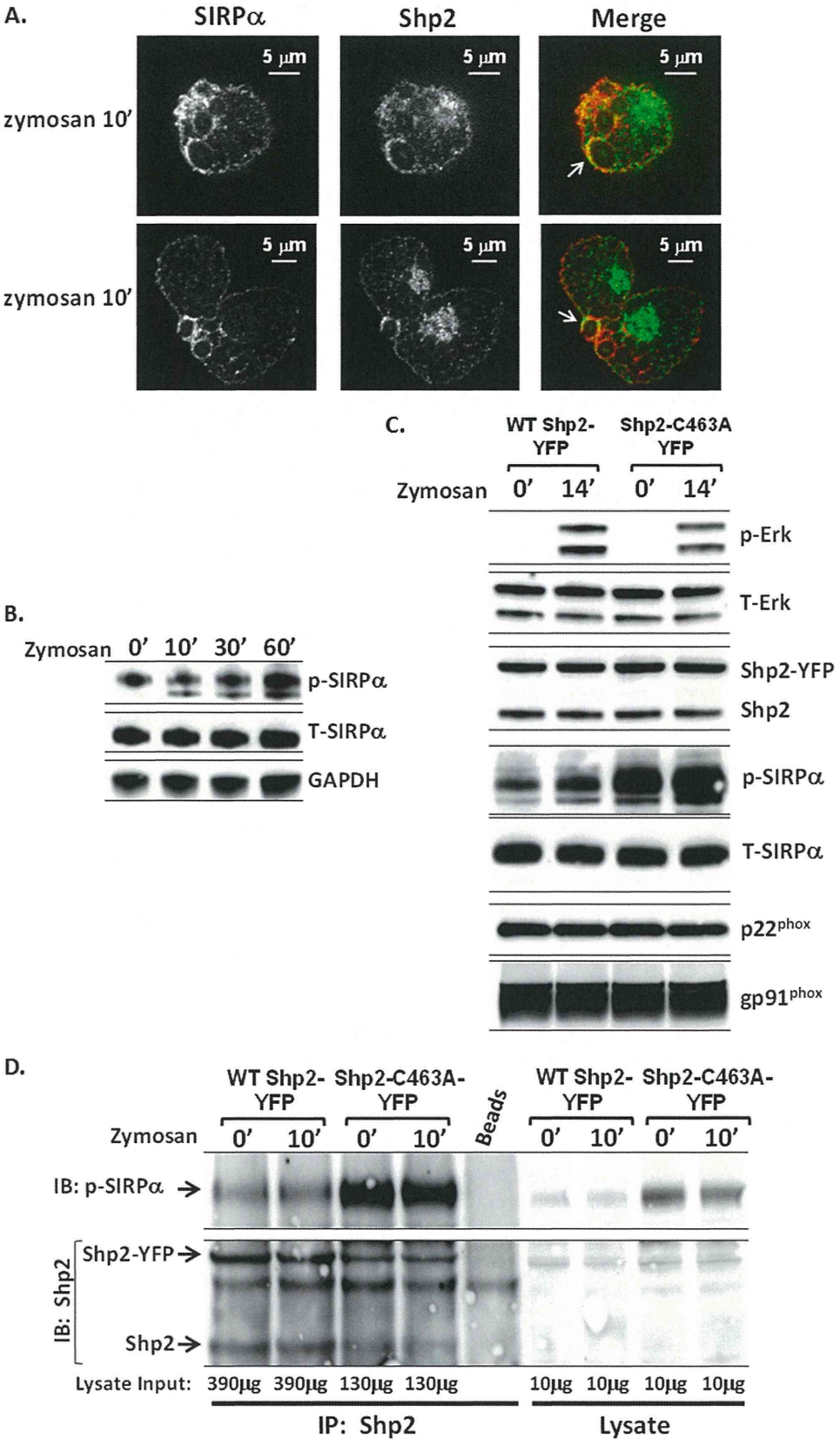

vated levels of phospho-SIRPα correlated to reduced levels of phospho-Erk (Fig. 7*C*), suggesting that Shp2 dephosphorylation of SIRPα constrains the SIRPα inhibitory function to permit normal Erk activation.

These findings support a model whereby Shp2 interacts with phosphorylated SIRPα and in which Shp2, upon SIRPα dephosphorylation, is released and available to augment activation of the Ras-Erk pathway, promote association of the NADPH oxidase protein complex, and enhance production of ROS. To address this hypothesis, we performed co-IP assays to examine the interaction between phospho-SIRPα and WT Shp2 compared with Shp2-C463A. Although we did observe an interaction between WT Shp2 and phospho-SIRPα (Fig. 7*D*), this interaction was in fact difficult to detect and required the use of ~3-fold more protein lysate for the co-IP compared with the amount of lysate used to detect the very strong interaction between Shp2-C463A and phospho-SIRPα (Fig. 7*D*). The modest biochemical interaction observed between WT Shp2 and phospho-SIRPα is consistent with the relatively low number of phagosomes demonstrating WT Shp2-SIRPα co-localization upon zymosan stimulation (Fig. 7*A*) and supports the notion that Shp2 dephosphorylation of SIRPα and disruption of the Shp2-SIRPα interaction is needed for optimal activation of Erk and NADPH oxidase.

DISCUSSION

Innate immune cell production of microbicidal ROS in response to foreign stimuli is vital for clearance of invading pathogens and immunocompetence. However, ROS production needs to be regulated in a temporal and spatial manner to minimize nonspecific damage to healthy tissues. Within this manuscript, we have demonstrated that the protein-tyrosine phosphatase, Shp2, is a novel player in the Dectin-1-stimulated signaling pathway and functions downstream of Syk and upstream of Erk to promote NADPH oxidase activation and oxidative burst. Further, we found that Shp2 activation and dephosphorylation of the inhibitory immunoreceptor, SIRPα, correlates kinetically with peak ROS production in Dectin-1-stimulated macrophages.

Shp2 is highly expressed in hematopoietic cells and has previously been shown to promote IL-6 production by promoting activation of NFκB (45). Additionally, Shp2 has been shown to be an important component of the leptin receptor signaling pathway in protecting against the parasite *E. histolytica*, and a component of this protection is due to STAT3-regulated IL-6 production (12). However, the role of Shp2 in oxidative burst has never been described. We first found that cells bearing genetic disruption of *Ptpn11* produce lower levels of zymosan- and SOZ-stimulated ROS. Using a series of Shp2 point mutants, we found that both the N-SH2 domain and the phosphatase domain of Shp2 are needed for zymosan- and SOZ-stimulated ROS. Importantly, videomicroscopy demonstrated that Shp2-R32K (N-SH2 domain mutant) failed to be recruited to the phagosome, whereas phosphatase dead Shp2-C463A was strongly recruited to phagosomes and was retained more intensely than WT Shp2 (Fig. 3*G*). These findings indicate that the N-SH2 domain is needed for Shp2 recruitment to the phagosome; however, once recruited, the phosphatase function of Shp2 is needed to promote ROS production. Supporting this idea, GOF Shp2 mutants Shp2-D61Y and Shp2-E76K increased both zymosan- and SOZ-stimulated ROS (Figs. 4 and 5).

Given the apparent positive functional role of Shp2 phosphatase on ROS production and the kinetic correlation of Erk activation with maximal ROS production (Fig. 1, *A* and *B*), we reasoned that Shp2 exerts its positive effect on NADPH oxidase activation via positive regulation of Erk, because Shp2 has been shown to positively up-regulate Erk activation in response to multiple stimuli (34, 46, 47). This notion is consistent with previous studies that have demonstrated positive regulation of Erk activation on NADPH oxidase (38–40). We found that the Erk inhibitor, SCH772984, reduced ROS production in both WT cells and in cells expressing GOF Shp2D61Y (Fig. 6), placing Erk downstream of Shp2 and upstream ROS production.

We next interrogated potential Shp2 substrates that may be involved in the regulation of particulate-stimulated Erk activation and ROS production. SIRPα, also known as SHPS-1/BIT/CD172a, was first identified as a phosphorylated glycoprotein that interacted with Shp2 in response to insulin stimulation, and expression of catalytically inactive Shp2 resulted in increased tyrosine phosphorylation of SIRPα (48). SIRPα contains extracellular immunoglobulin-like domains and four intracellular tyrosine residues followed by amino acid sequence *XX*(L/V/I), indicating sites of tyrosine phosphorylation (43). Several studies indicate that SIRPα may be a physiological substrate for Shp2 (42, 43). Early functional studies in fibroblasts indicated that overexpression of SIRPα inhibited receptor tyrosine kinase- and cytokine receptor-stimulated cell proliferation and that the intracellular tyrosine residues were vital for the SIRPα inhibitory function (42). Given the high expression level of SIRPα in macrophages, investigators found that SIRPα negatively modulates inflammatory cytokine production via down-regulation of NFκB-regulated expression (19, 49). Additionally, one study found that SIRPα phosphorylation functioned to inhibit soluble stimulation (phorbol 12-myristate 13-acetate)-induced plasma membrane ROS by down-regulating expression of the NADPH oxidase component, gp91^{phox} (44).

FIGURE 7. **SIRPα phosphorylation and interaction with Shp2 in zymosan-stimulated WT Shp2- and Shp2-C463A-expressing BMMs.** *A*, co-localization of SIRPα and Shp2 in WT mouse PEMs 10 min after zymosan-induced phagocytosis and immunofluorescent staining with anti-SIRPα (catalog no. 53721; Abcam) and anti-Shp2 (BD Biosciences; catalog no. 610621) and Alexa Fluor 568 goat anti-rabbit IgG and goat 488 anti-mouse IgG1, respectively. *B*, immunoblot demonstrating reduced levels of phospho-SIRPα upon zymosan stimulation of WT PEMs. *C*, phosphorylation of SIRPα and Erk in BMMs retrovirally transduced with YFP-WT Shp2 or YFP-Shp2-C463A. Total Shp2, SIRPα, Erk, p22^{phox}, and gp91^{phox} were also examined using antibodies described under "Experimental Procedures." *D*, binding of WT Shp2 and Shp2-C463A mutant to tyrosine-phosphorylated SIRPα in macrophages before and after zymosan stimulation. Cell lysates from macrophages expressing YFP-WT Shp2 or YFP-Shp2-C463A were subjected to IP anti-Shp2 antibody (SC-280; Santa Cruz Biotechnology) followed by immunoblotting (*IB*) with anti-phospho-SIRPα or anti-Shp2 (catalog no. 610621; BD Biosciences). 390 μg of protein lysis from macrophages expressing YFP-WT Shp2 and 130 μg of protein lysis from macrophages expressing YFP-Shp2-C463A were used for IP. 10 μg of protein lysis was used to do immunoblot analysis. The data are representative of three separate experiments.

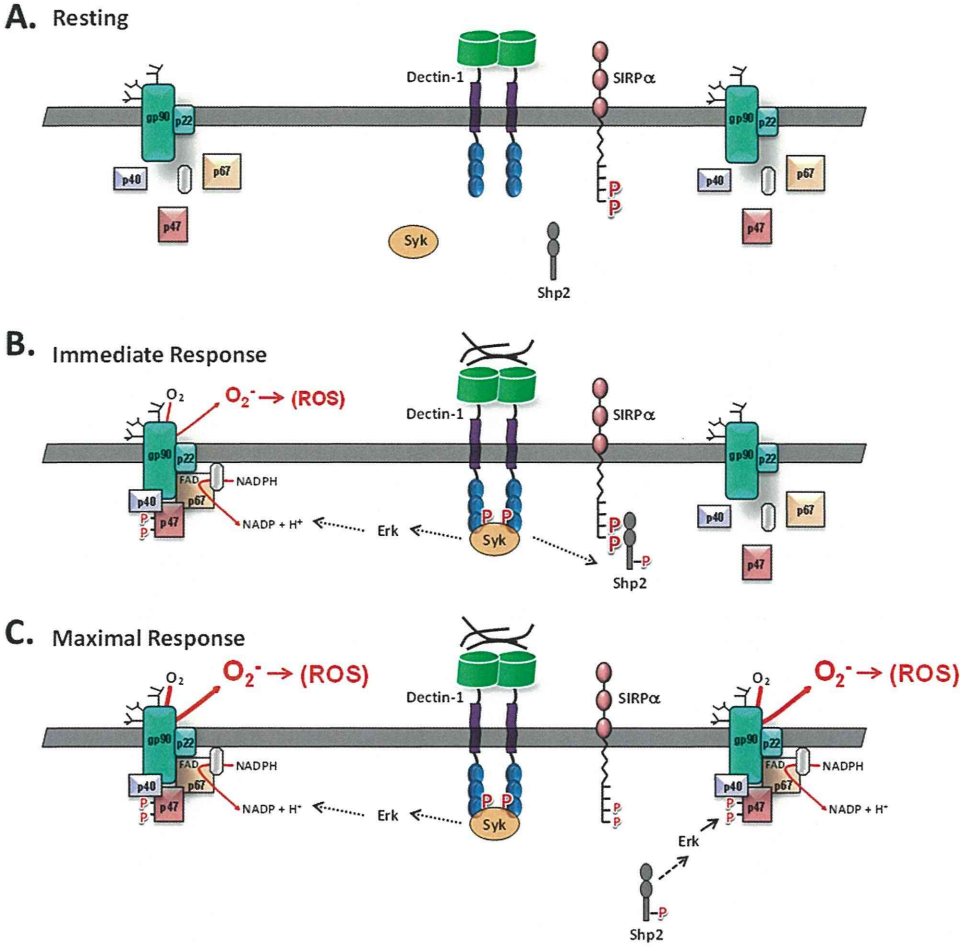

FIGURE 8. **Schematic diagram indicating proposed mechanism of Shp2 and SIRPα interaction in response to Dectin-1 stimulation.** *A*, cells at resting state. *B*, immediate Dectin-1-stimulated ROS production in a Syk-dependent, Shp2-independent manner. *C*, following Shp2 dephosphorylation of SIRPα, maximal Dectin-1-stimulated ROS is produced in both a Syk-dependent and Shp2-dependent manner.

To date, however, no previous studies have identified SIRPα as an important regulatory molecule in particulate-stimulated oxidative burst. We first defined that SIRPα is indeed present on early phagosomal membranes in response to zymosan stimulation with similar kinetics to Shp2 phagosomal recruitment. In fluorescent microscopy studies, however, although we found that Shp2 and SIRPα co-localize on the early phagosome (Fig. 7*A*), we were surprised to find that the co-localization was modest and seen in only ~10–15% of phagosomes at the time corresponding to maximal ROS production (10 min poststimulation). These findings suggest that SIRPα phosphorylation recruits Shp2 to the phagosome membrane and that the Shp2-SIRPα interaction delays the full oxidative burst by sequestering Shp2 from the Ras-Erk pathway, thus deferring maximal Erk activation and ROS production. The increased association of phosphatase-dead Shp2-C463A with the phagosome (Fig. 3*G*) and the increased biochemical interaction between Shp2-C463A and SIRPα (Fig. 7*D*) in conjunction with reduced ROS production support this model.

Although our data support a positive role for Shp2 phosphatase in particulate-stimulated ROS production by dephosphorylating and thus repressing the inhibitory role of SIRPα, it is important to put these findings into context with previous studies in this signaling pathway. First, studies from the Eklund lab demonstrated that Shp2 functions to dephosphorylate the transcription factors ICSBP and HoxA10, resulting in reduced transcription and expression of the NADPH oxidase protein components gp91^{phox} and p67^{phox} (14, 15). These studies very nicely provide a rational mechanism of how GOF Shp2 mutants may inhibit expression of genes needed for myeloid cell terminal differentiation and thus promote leukemogenesis.

Additionally, van Beek *et al.* (44) demonstrated that ectopic expression of SIRPα in PLB-985 cells functioned in an inhibitory manner by repressing gp91^{phox} expression during granulocytic or monocytic differentiation, leading to reduced soluble stimulation (phorbol 12-myristate 13-acetate)-induced ROS. Notably, these previous studies were performed in undifferentiated or differentiating myeloid cells, whereas our studies were performed in terminally differentiated macrophages. Importantly, in terminally differentiated macrophages, we did not find a difference in expression of the various NADPH oxidase components in cells lacking Shp2 (Fig. 2), expressing loss of function Shp2 mutants (Fig. 3), or gain of function Shp2 mutants (Figs. 4 and 5). Contrasting our studies to this previous work highlights an interesting concept that in undifferentiated myeloid cells, Shp2 and SIRPα may be more important for regulating transcription factor function and myeloid cell differentiation (50, 51), whereas in terminally differentiated cells, Shp2 and SIRPα are more impor-

tant for regulating phosphorylation and subcellular localization, respectively, of cytoplasmic signaling proteins.

Further, whereas many studies focus on the inhibitory role of SIRPα in myeloid cell immune function, others have found that SIRPα can also play a positive role in immune cell function (52). Importantly, this positive regulatory role of SIRPα was found in the context of Shp1-expressing hematopoietic cells, whereas many of the original studies defining a negative regulatory role of SIRPα were performed in fibroblasts which express only Shp2 (52). Because both Shp1 and Shp2 are expressed in hematopoietic cells and have both been found to interact with SIRPα and because Shp1 is conventionally thought to play a negative regulatory role and Shp2 is thought to play a positively regulatory role in hematopoietic cell function, these considerations bring into relief the speculative idea that Shp1 may function to dephosphorylate and inhibit the positive regulatory role of SIRPα (leading to a net negative signal), whereas Shp2 may function to dephosphorylate and inhibit the negative regulatory role of SIRPα (leading to a net positive signal). Although beyond the point of the current study, it may be of interest to compare the effect of phosphatase dead Shp1 with that of phosphatase dead Shp2 in particulate-stimulated ROS production in terminally differentiated macrophages or neutrophils.

Based on our findings within the current study, we have clarified a model that places Shp2 activation downstream of Dectin-1-stimulated Syk and upstream of Erk and ROS production (Fig. 8). Previous work defined that upon stimulation, Dectin-1 is phosphorylated (likely by members of the Src family of kinases) resulting in Syk recruitment, Ras-Erk pathway activation (16), and immediate production of ROS (Fig. 8, *A* and *B*). Findings within this study demonstrate that Dectin-1 stimulation leads to activation of Shp2 in a Syk-dependent manner and that phospho-Shp2 is recruited to phosphorylated SIRPα (Fig. 8*B*). Once Shp2 dephosphorylates SIRPα, Shp2 is available for additional positive regulation of the Ras-Erk pathway, leading to maximal ROS production (Fig. 8*C*). A potential means of Erk activation of NADPH oxidase function is phosphorylation of $p47^{phox}$, which has been found previously in neutrophils (40, 53). It is possible that the SIRPα interaction with Shp2 defers maximal ROS production for the purpose of mitigating or preventing unwarranted ROS release to normal tissues. These findings also have application for improved understanding of the childhood leukemia, juvenile myelomonocytic leukemia, because aberrantly elevated ROS production from activating *PTPN11*-expressing innate immune cells may account for the common difficulty in clinically differentiating juvenile myelomonocytic leukemia from microbial and viral infections (54–56). Collectively, our findings demonstrate that Shp2 positively regulates oxidative burst at least in part by promoting Erk activation and that the Shp2-SIRPα interaction may fine tune the optimal timing and location for ROS production.

Acknowledgments—We thank Dr. Jesaitis for antibodies 54.1 against $gp91^{phox}$ and NS2 against $p22^{phox}$. We also thank the Indiana University Simon Cancer Center Flow Cytometry Core and Indiana Center for Biological Microscopy. We gratefully acknowledge the administrative assistance of Marilyn L. Wales.

REFERENCES

1. Minakami, R., and Sumimotoa, H. (2006) Phagocytosis-coupled activation of the superoxide-producing phagocyte oxidase, a member of the NADPH oxidase (nox) family. *Int. J. Hematol.* **84,** 193–198
2. Groemping, Y., and Rittinger, K. (2005) Activation and assembly of the NADPH oxidase: a structural perspective. *Biochem. J.* **386,** 401–416
3. Nauseef, W. M. (2004) Assembly of the phagocyte NADPH oxidase. *Histochem. Cell Biol.* **122,** 277–291
4. Dinauer, M. C. (2005) Chronic granulomatous disease and other disorders of phagocyte function. *Hematology Am. Soc. Hematol. Educ. Program,* 89–95
5. Stasia, M. J., and Li, X. J. (2008) Genetics and immunopathology of chronic granulomatous disease. *Semin. Immunopathol.* **30,** 209–235
6. Qu, C. K., Shi, Z. Q., Shen, R., Tsai, F. Y., Orkin, S. H., and Feng, G. S. (1997) A deletion mutation in the SH2-N domain of Shp-2 severely suppresses hematopoietic cell development. *Mol. Cell Biol.* **17,** 5499–5507
7. Qu, C. K., Yu, W. M., Azzarelli, B., Cooper, S., Broxmeyer, H. E., and Feng, G. S. (1998) Biased suppression of hematopoiesis and multiple developmental defects in chimeric mice containing Shp-2 mutant cells. *Mol. Cell Biol.* **18,** 6075–6082
8. Chan, G., Cheung, L. S., Yang, W., Milyavsky, M., Sanders, A. D., Gu, S., Hong, W. X., Liu, A. X., Wang, X., Barbara, M., Sharma, T., Gavin, J., Kutok, J. L., Iscove, N. N., Shannon, K. M., Dick, J. E., Neel, B. G., and Braun, B. S. (2011) Essential role for Ptpn11 in survival of hematopoietic stem and progenitor cells. *Blood* **117,** 4253–4261
9. Zhu, H. H., Ji, K., Alderson, N., He, Z., Li, S., Liu, W., Zhang, D. E., Li, L., and Feng, G. S. (2011) Kit-Shp2-Kit signaling acts to maintain a functional hematopoietic stem and progenitor cell pool. *Blood* **117,** 5350–5361
10. Tartaglia, M., Niemeyer, C. M., Fragale, A., Song, X., Buechner, J., Jung, A., Hählen, K., Hasle, H., Licht, J. D., and Gelb, B. D. (2003) Somatic mutations in PTPN11 in juvenile myelomonocytic leukemia, myelodysplastic syndromes and acute myeloid leukemia. *Nat. Genet.* **34,** 148–150
11. Tartaglia, M., Mehler, E. L., Goldberg, R., Zampino, G., Brunner, H. G., Kremer, H., van der Burgt, I., Crosby, A. H., Ion, A., Jeffery, S., Kalidas, K., Patton, M. A., Kucherlapati, R. S., and Gelb, B. D. (2001) Mutations in PTPN11, encoding the protein tyrosine phosphatase SHP-2, cause Noonan syndrome. *Nat. Genet.* **29,** 465–468
12. Mackey-Lawrence, N. M., and Petri, W. A., Jr. (2012) Leptin and mucosal immunity. *Mucosal Immunol.* **5,** 472–479
13. Farooqi, I. S., Wangensteen, T., Collins, S., Kimber, W., Matarese, G., Keogh, J. M., Lank, E., Bottomley, B., Lopez-Fernandez, J., Ferraz-Amaro, I., Dattani, M. T., Ercan, O., Myhre, A. G., Retterstol, L., Stanhope, R., Edge, J. A., McKenzie, S., Lessan, N., Ghodsi, M., De Rosa, V., Perna, F., Fontana, S., Barroso, I., Undlien, D. E., and O'Rahilly, S. (2007) Clinical and molecular genetic spectrum of congenital deficiency of the leptin receptor. *N. Engl. J. Med.* **356,** 237–247
14. Lindsey, S., Huang, W., Wang, H., Horvath, E., Zhu, C., and Eklund, E. A. (2007) Activation of SHP2 protein-tyrosine phosphatase increases HoxA10-induced repression of the genes encoding gp91(PHOX) and p67(PHOX). *J. Biol. Chem.* **282,** 2237–2249
15. Zhu, C., Lindsey, S., Konieczna, I., and Eklund, E. A. (2008) Constitutive activation of SHP2 protein tyrosine phosphatase inhibits ICSBP-induced transcription of the gene encoding gp91PHOX during myeloid differentiation. *J. Leukoc. Biol.* **83,** 680–691
16. Goodridge, H. S., Underhill, D. M., and Touret, N. (2012) Mechanisms of Fc receptor and dectin-1 activation for phagocytosis. *Traffic* **13,** 1062–1071
17. Cunha, C., Di Ianni, M., Bozza, S., Giovannini, G., Zagarella, S., Zelante, T., D'Angelo, C., Pierini, A., Pitzurra, L., Falzetti, F., Carotti, A., Perruccio, K., Latgé, J. P., Rodrigues, F., Velardi, A., Aversa, F., Romani, L., and Carvalho, A. (2010) Dectin-1 Y238X polymorphism associates with susceptibility to invasive aspergillosis in hematopoietic transplantation through impairment of both recipient- and donor-dependent mechanisms of antifungal immunity. *Blood* **116,** 5394–5402
18. Ferwerda, B., Ferwerda, G., Plantinga, T. S., Willment, J. A., van Spriel, A. B., Venselaar, H., Elbers, C. C., Johnson, M. D., Cambi, A., Huysamen, C., Jacobs, L., Jansen, T., Verheijen, K., Masthoff, L., Morré, S. A., Vriend,

G., Williams, D. L., Perfect, J. R., Joosten, L. A., Wijmenga, C., van der Meer, J. W., Adema, G. J., Kullberg, B. J., Brown, G. D., and Netea, M. G. (2009) Human dectin-1 deficiency and mucocutaneous fungal infections. *N. Engl. J. Med.* **361,** 1760–1767

19. Miyake, A., Murata, Y., Okazawa, H., Ikeda, H., Niwayama, Y., Ohnishi, H., Hirata, Y., and Matozaki, T. (2008) Negative regulation by SHPS-1 of Toll-like receptor-dependent proinflammatory cytokine production in macrophages. *Genes Cells* **13,** 209–219
20. Taylor, R. M., Burritt, J. B., Baniulis, D., Foubert, T. R., Lord, C. I., Dinauer, M. C., Parkos, C. A., and Jesaitis, A. J. (2004) Site-specific inhibitors of NADPH oxidase activity and structural probes of flavocytochrome b: characterization of six monoclonal antibodies to the p22phox subunit. *J. Immunol.* **173,** 7349–7357
21. Chan, G., Kalaitzidis, D., Usenko, T., Kutok, J. L., Yang, W., Mohi, M. G., and Neel, B. G. (2009) Leukemogenic Ptpn11 causes fatal myeloproliferative disorder via cell-autonomous effects on multiple stages of hematopoiesis. *Blood* **113,** 4414–4424
22. Zhang, E. E., Chapeau, E., Hagihara, K., and Feng, G. S. (2004) Neuronal Shp2 tyrosine phosphatase controls energy balance and metabolism. *Proc. Natl. Acad. Sci. U.S.A.* **101,** 16064–16069
23. Chan, R. J., Leedy, M. B., Munugalavadla, V., Voorhorst, C. S., Li, Y., Yu, M., and Kapur, R. (2005) Human somatic PTPN11 mutations induce hematopoietic-cell hypersensitivity to granulocyte-macrophage colony-stimulating factor. *Blood* **105,** 3737–3742
24. Li, X. J., Marchal, C. C., Stull, N. D., Stahelin, R. V., and Dinauer, M. C. (2010) p47phox Phox homology domain regulates plasma membrane but not phagosome neutrophil NADPH oxidase activation. *J. Biol. Chem.* **285,** 35169–35179
25. Zeng, M. Y., Pham, D., Bagaitkar, J., Liu, J., Otero, K., Shan, M., Wynn, T. A., Brombacher, F., Brutkiewicz, R. R., Kaplan, M. H., and Dinauer, M. C. (2013) An efferocytosis-induced, IL-4-dependent macrophage-iNKT cell circuit suppresses sterile inflammation and is defective in murine CGD. *Blood* **121,** 3473–3483
26. Li, X. J., Tian, W., Stull, N. D., Grinstein, S., Atkinson, S., and Dinauer, M. C. (2009) A fluorescently tagged C-terminal fragment of p47phox detects NADPH oxidase dynamics during phagocytosis. *Mol. Biol. Cell* **20,** 1520–1532
27. Matute, J. D., Arias, A. A., Wright, N. A., Wrobel, I., Waterhouse, C. C., Li, X. J., Marchal, C. C., Stull, N. D., Lewis, D. B., Steele, M., Kellner, J. D., Yu, W., Meroueh, S. O., Nauseef, W. M., and Dinauer, M. C. (2009) A new genetic subgroup of chronic granulomatous disease with autosomal recessive mutations in p40 phox and selective defects in neutrophil NADPH oxidase activity. *Blood* **114,** 3309–3315
28. Suh, C. I., Stull, N. D., Li, X. J., Tian, W., Price, M. O., Grinstein, S., Yaffe, M. B., Atkinson, S., and Dinauer, M. C. (2006) The phosphoinositide-binding protein p40phox activates the NADPH oxidase during FcgammaIIA receptor-induced phagocytosis. *J. Exp. Med.* **203,** 1915–1925
29. Greenberg, S., Burridge, K., and Silverstein, S. C. (1990) Colocalization of F-actin and talin during Fc receptor-mediated phagocytosis in mouse macrophages. *J. Exp. Med.* **172,** 1853–1856
30. Tian, W., Li, X. J., Stull, N. D., Ming, W., Suh, C. I., Bissonnette, S. A., Yaffe, M. B., Grinstein, S., Atkinson, S. J., and Dinauer, M. C. (2008) Fc gamma R-stimulated activation of the NADPH oxidase: phosphoinositide-binding protein p40phox regulates NADPH oxidase activity after enzyme assembly on the phagosome. *Blood* **112,** 3867–3877
31. Ellson, C. D., Davidson, K., Ferguson, G. J., O'Connor, R., Stephens, L. R., and Hawkins, P. T. (2006) Neutrophils from p40phox−/− mice exhibit severe defects in NADPH oxidase regulation and oxidant-dependent bacterial killing. *J. Exp. Med.* **203,** 1927–1937
32. Goodwin, C. B., Yang, Z., Yin, F., Yu, M., and Chan, R. J. (2012) Genetic disruption of the PI3K regulatory subunits, p85alpha, p55alpha, and p50alpha, normalizes mutant PTPN11-induced hypersensitivity to GM-CSF. *Haematologica* **97,** 1042–1047
33. Yang, Z., Kondo, T., Voorhorst, C. S., Nabinger, S. C., Ndong, L., Yin, F., Chan, E. M., Yu, M., Würstlin, O., Kratz, C. P., Niemeyer, C. M., Flotho, C., Hashino, E., and Chan, R. J. (2009) Increased c-Jun expression and reduced GATA2 expression promote aberrant monocytic differentiation induced by activating PTPN11 mutants. *Mol. Cell Biol.* **29,** 4376–4393
34. Neel, B. G., Gu, H., and Pao, L. (2003) The 'Shp'ing news: SH2 domain-containing tyrosine phosphatases in cell signaling. *Trends Biochem. Sci.* **28,** 284–293
35. Gu, H., Botelho, R. J., Yu, M., Grinstein, S., and Neel, B. G. (2003) Critical role for scaffolding adapter Gab2 in Fc gamma R-mediated phagocytosis. *J. Cell Biol.* **161,** 1151–1161
36. Keilhack, H., David, F. S., McGregor, M., Cantley, L. C., and Neel, B. G. (2005) Diverse biochemical properties of Shp2 mutants. Implications for disease phenotypes. *J. Biol. Chem.* **280,** 30984–30993
37. Guyton, K. Z., Liu, Y., Gorospe, M., Xu, Q., and Holbrook, N. J. (1996) Activation of mitogen-activated protein kinase by H2O2. Role in cell survival following oxidant injury. *J. Biol. Chem.* **271,** 4138–4142
38. Torres, M., and Forman, H. J. (1999) Activation of several MAP kinases upon stimulation of rat alveolar macrophages: role of the NADPH oxidase. *Arch. Biochem. Biophys.* **366,** 231–239
39. Laplante, M. A., Wu, R., El Midaoui, A., and de Champlain, J. (2003) NAD(P)H oxidase activation by angiotensin II is dependent on p42/44 ERK-MAPK pathway activation in rat's vascular smooth muscle cells. *J. Hypertens.* **21,** 927–936
40. Makni-Maalej, K., Chiandotto, M., Hurtado-Nedelec, M., Bedouhene, S., Gougerot-Pocidalo, M. A., Dang, P. M., and El-Benna, J. (2013) Zymosan induces NADPH oxidase activation in human neutrophils by inducing the phosphorylation of p47phox and the activation of Rac2: involvement of protein tyrosine kinases, PI3Kinase, PKC, ERK1/2 and p38MAPkinase. *Biochem. Pharmacol.* **85,** 92–100
41. Pollock, J. D., Williams, D. A., Gifford, M. A., Li, L. L., Du, X., Fisherman, J., Orkin, S. H., Doerschuk, C. M., and Dinauer, M. C. (1995) Mouse model of X-linked chronic granulomatous disease, an inherited defect in phagocyte superoxide production. *Nat. Genet.* **9,** 202–209
42. Kharitonenkov, A., Chen, Z., Sures, I., Wang, H., Schilling, J., and Ullrich, A. (1997) A family of proteins that inhibit signalling through tyrosine kinase receptors. *Nature* **386,** 181–186
43. Fujioka, Y., Matozaki, T., Noguchi, T., Iwamatsu, A., Yamao, T., Takahashi, N., Tsuda, M., Takada, T., and Kasuga, M. (1996) A novel membrane glycoprotein, SHPS-1, that binds the SH2-domain-containing protein tyrosine phosphatase SHP-2 in response to mitogens and cell adhesion. *Mol. Cell Biol.* **16,** 6887–6899
44. van Beek, E. M., Zarate, J. A., van Bruggen, R., Schornagel, K., Tool, A. T., Matozaki, T., Kraal, G., Roos, D., and van den Berg, T. K. (2012) SIRPalpha controls the activity of the phagocyte NADPH oxidase by restricting the expression of gp91(phox). *Cell Reports* **2,** 748–755
45. You, M., Flick, L. M., Yu, D., and Feng, G. S. (2001) Modulation of the nuclear factor kappa B pathway by Shp-2 tyrosine phosphatase in mediating the induction of interleukin (IL)-6 by IL-1 or tumor necrosis factor. *J. Exp. Med.* **193,** 101–110
46. Chan, R. J., and Feng, G. S. (2007) PTPN11 is the first identified proto-oncogene that encodes a tyrosine phosphatase. *Blood* **109,** 862–867
47. Liu, X., and Qu, C. K. (2011) Protein tyrosine phosphatase SHP-2 (PTPN11) in hematopoiesis and leukemogenesis. *J. Signal Transduct.* **2011,** 195239
48. Noguchi, T., Matozaki, T., Fujioka, Y., Yamao, T., Tsuda, M., Takada, T., and Kasuga, M. (1996) Characterization of a 115-kDa protein that binds to SH-PTP2, a protein-tyrosine phosphatase with Src homology 2 domains, in Chinese hamster ovary cells. *J. Biol. Chem.* **271,** 27652–27658
49. Kong, X. N., Yan, H. X., Chen, L., Dong, L. W., Yang, W., Liu, Q., Yu, L. X., Huang, D. D., Liu, S. Q., Liu, H., Wu, M. C., and Wang, H. Y. (2007) LPS-induced down-regulation of signal regulatory protein α contributes to innate immune activation in macrophages. *J. Exp. Med.* **204,** 2719–2731
50. Huang, H., Woo, A. J., Waldon, Z., Schindler, Y., Moran, T. B., Zhu, H. H., Feng, G. S., Steen, H., and Cantor, A. B. (2012) A Src family kinase-Shp2 axis controls RUNX1 activity in megakaryocyte and T-lymphocyte differentiation. *Genes Dev.* **26,** 1587–1601
51. Nabinger, S. C., Li, X. J., Ramdas, B., He, Y., Zhang, X., Zeng, L., Richine, B., Bowling, J. D., Fukuda, S., Goenka, S., Liu, Z., Feng, G. S., Yu, M., Sandusky, G. E., Boswell, H. S., Zhang, Z. Y., Kapur, R., and Chan, R. J. (2013) The protein tyrosine phosphatase, Shp2, positively contributes to FLT3-ITD-induced hematopoietic progenitor hyperproliferation and malignant disease *in vivo*. *Leukemia* **27,** 398–408

52. Alblas, J., Honing, H., de Lavalette, C. R., Brown, M. H., Dijkstra, C. D., and van den Berg, T. K. (2005) Signal regulatory protein alpha ligation induces macrophage nitric oxide production through JAK/STAT- and phosphatidylinositol 3-kinase/Rac1/NAPDH oxidase/H2O2-dependent pathways. *Mol. Cell. Biol.* **25,** 7181–7192
53. Dewas, C., Fay, M., Gougerot-Pocidalo, M. A., and El-Benna, J. (2000) The mitogen-activated protein kinase extracellular signal-regulated kinase 1/2 pathway is involved in formyl-methionyl-leucyl-phenylalanine-induced p47phox phosphorylation in human neutrophils. *J. Immunol.* **165,** 5238–5244
54. Lorenzana, A., Lyons, H., Sawaf, H., Higgins, M., Carrigan, D., and Emanuel, P. D. (2002) Human herpesvirus 6 infection mimicking juvenile myelomonocytic leukemia in an infant. *J. Pediatr. Hematol. Oncol.* **24,** 136–141
55. Moritake, H., Ikeda, T., Manabe, A., Kamimura, S., and Nunoi, H. (2009) Cytomegalovirus infection mimicking juvenile myelomonocytic leukemia showing hypersensitivity to granulocyte-macrophage colony stimulating factor. *Pediatr. Blood Cancer* **53,** 1324–1326
56. Pinkel, D. (1998) Differentiating juvenile myelomonocytic leukemia from infectious disease. *Blood* **91,** 365–367

OPEN ACCESS Freely available online

PLOS | ONE

Comprehensive Behavioral Analysis of Cluster of Differentiation 47 Knockout Mice

Hisatsugu Koshimizu[1,2], Keizo Takao[2,3,4], Takashi Matozaki[5,6], Hiroshi Ohnishi[5,7]*, Tsuyoshi Miyakawa[1,2,3,4]*

1 Division of Systems Medical Science, Institute for Comprehensive Medical Science, Fujita Health University, Toyoake, Japan, **2** Core Research for Evolutional Science and Technology (CREST), Japan Science and Technology Agency, Kawaguchi, Japan, **3** Section of Behavior Patterns, Center for Genetic Analysis of Behavior, National Institute for Physiological Sciences, Okazaki, Japan, **4** Genetic Engineering and Functional Genomics Group, Frontier Technology Center, Kyoto University Graduate School of Medicine, Kyoto, Japan, **5** Laboratory of Biosignal Sciences, Institute for Molecular and Cellular Regulation, Gunma University, Maebashi, Japan, **6** Division of Molecular and Cellular Signaling, Department of Biochemistry and Molecular Biology, Kobe University Graduate School of Medicine, Kobe, Japan, **7** Department of Laboratory Sciences, Gunma University Graduate School of Health Sciences, Maebashi, Japan

Abstract

Cluster of differentiation 47 (CD47) is a member of the immunoglobulin superfamily which functions as a ligand for the extracellular region of signal regulatory protein α (SIRPα), a protein which is abundantly expressed in the brain. Previous studies, including ours, have demonstrated that both CD47 and SIRPα fulfill various functions in the central nervous system (CNS), such as the modulation of synaptic transmission and neuronal cell survival. We previously reported that CD47 is involved in the regulation of depression-like behavior of mice in the forced swim test through its modulation of tyrosine phosphorylation of SIRPα. However, other potential behavioral functions of CD47 remain largely unknown. In this study, in an effort to further investigate functional roles of CD47 in the CNS, CD47 knockout (KO) mice and their wild-type littermates were subjected to a battery of behavioral tests. CD47 KO mice displayed decreased prepulse inhibition, while the startle response did not differ between genotypes. The mutants exhibited slightly but significantly decreased sociability and social novelty preference in Crawley's three-chamber social approach test, whereas in social interaction tests in which experimental and stimulus mice have direct contact with each other in a freely moving setting in a novel environment or home cage, there were no significant differences between the genotypes. While previous studies suggested that CD47 regulates fear memory in the inhibitory avoidance test in rodents, our CD47 KO mice exhibited normal fear and spatial memory in the fear conditioning and the Barnes maze tests, respectively. These findings suggest that CD47 is potentially involved in the regulation of sensorimotor gating and social behavior in mice.

Citation: Koshimizu H, Takao K, Matozaki T, Ohnishi H, Miyakawa T (2014) Comprehensive Behavioral Analysis of Cluster of Differentiation 47 Knockout Mice. PLoS ONE 9(2): e89584. doi:10.1371/journal.pone.0089584

Editor: Ya-Ping Tang, Louisiana State University Health Sciences Center, United States of America

Received September 30, 2013; **Accepted** January 21, 2014; **Published** February 24, 2014

Funding: This research was supported by Grant-in-Aid for Scientific Research on Priority Areas (200163013), Grant-in-Aid for Exploratory Research (19653081), Grant-in-Aid for Scientific Research (B) (21300121), Grant-in-Aid for Scientific Research (C) (23500437), Scientific Research on Innovative Areas ("Brain Environment", 24111546 and 24111508), Grant-in-Aid for Scientific Research on Innovative Areas (Comprehensive Brain Science Network), and Integrative Brain Research (IBR- shien) from the Ministry of Education, Culture, Sports, Science, and Technology (MEXT) of Japan, and grants from Core Research for Evolutional Science and Technology (CREST) and the Institute for Bioinformatics Research and Development (BIRD) of the Japan Science and Technology Agency (JST). The funders had no role in study design, data collection and analysis, decision to publish, or preparation of the manuscript.

Competing Interests: The authors have declared that no competing interests exist.

* E-mail: ohnishih@gunma-u.ac.jp (HO); miyakawa@fujita-hu.ac.jp (TM)

Background

Cluster of differentiation 47 (CD47), also referred to as integrin-associated protein (IAP), is a member of the immunoglobulin superfamily possessing a V-type immunoglobulin domain in its extracellular domain, five membrane-spanning domains and a short cytoplasmic tail [1]. CD47 functions as a ligand for the extracellular region of the transmembrane protein known as signal regulatory protein α (SIRPα; also known as SHPS-1, p84, and BIT) [2,3]. SIRPα contains three Ig-like domains in its extracellular region and putative tyrosine phosphorylation sites in its cytoplasmic region [3,4]. CD47 is expressed throughout the brain, with the regions in which it is abundant overlapping extensively with those enriched in SIRPα [5–7]. CD47 and SIRPα are both highly expressed in synapse-rich regions [2,4,6], and are considered to form a heterophilic complex to mediate bi-directional signaling between cells [2,8,9]. Binding of CD47 to SIRPα is required for the tyrosine phosphorylation of SIRPα [10], which is regulated by various receptor-type tyrosine kinases, including tropomyosin-related kinase B (TrkB), as well as the Src family kinases (SFKs) [4]. When SIRPα is phosphorylated, it then activates Src homology 2 domain–containing protein tyrosine phosphatase (Shp2) [11,12], which is known to be involved in central nervous system (CNS) cell survival, differentiation, and cellular morphogenesis [13–15].

Our previous *in vitro* studies indicate that CD47 and SIRPα are involved in the regulation of brain-derived neurotrophic factor (BDNF)-dependent cell survival of CNS neurons, including cerebral cortical neurons, cerebellar granule neurons, and ventral mesencephalic dopaminergic neurons [16–19]. We also revealed that endogenous SIRPα is expressed at the surface of both axons and dendrites of cultured hippocampal neurons, and that endogenous CD47 is localized predominantly to the surface of

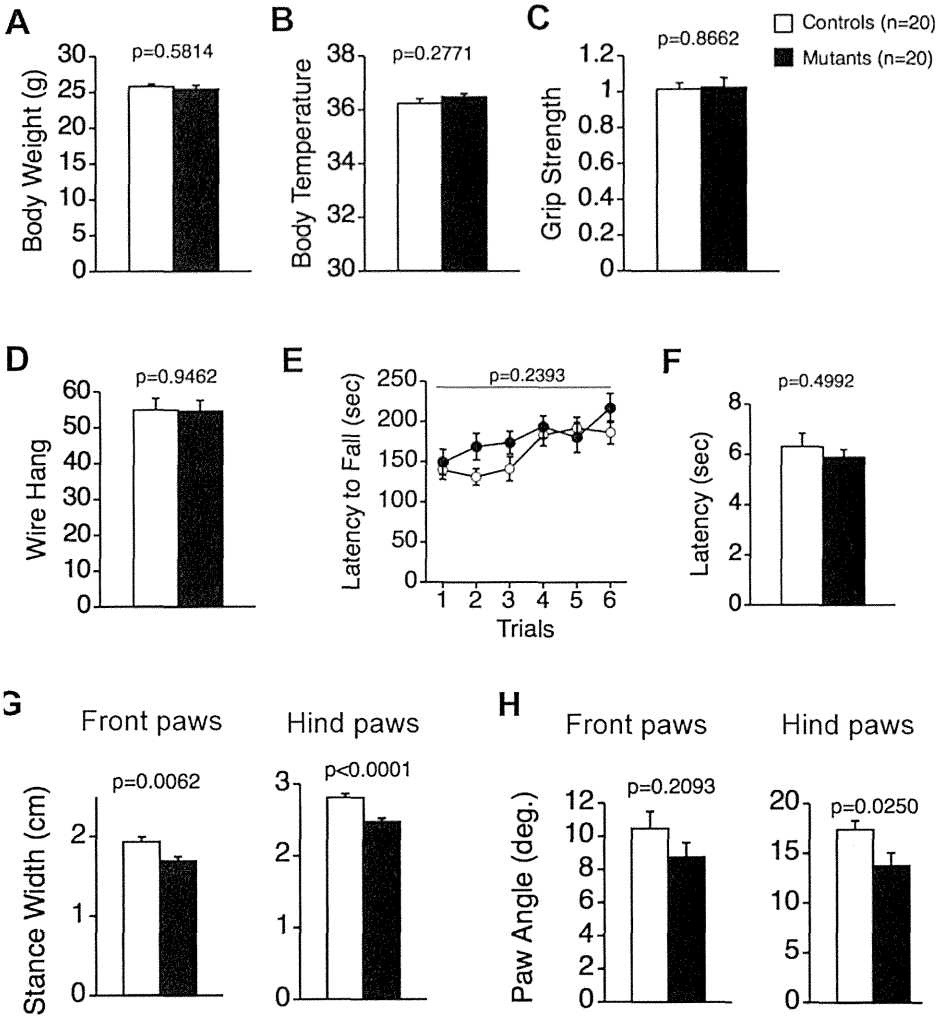

Figure 1. Physical characteristics, neuromuscular strength, motor coordination, nociception, and gait in CD47 KO and wild-type mice. No significant differences between genotypes were detected in body weight (A), body temperature (B), grip strength (C), or latency to fall in the wire hang test (D). (E) Likewise, no significant differences between the genotypes were observed in latency to fall from the rotarod (F) or latency to the first paw response in the hot plate test. CD47 KO mice, n = 20; wild-type mice, n = 20. (G–H) CD47 KO mice were also subjected to gait analysis. (G) The mutants showed significant decreases in stance width for front and hind paws compared to wild-type mice. (H) Paw angles for hind paws, but not for front paws, were significantly narrower in the mutants than in wild-type mice. CD47 KO mice, n = 19; wild-type mice, n = 20.
doi:10.1371/journal.pone.0089584.g001

dendrites [7]. Overexpression of CD47 and SIRPα in cultured mouse hippocampal neurons resulted in marked accumulation of those molecules at sites of contact between CD47-expressing dendrites and SIRPα-expressing axons [7]. In addition, expression of CD47 induced the phosphorylation of extracellular-signal-regulated kinase (ERK), which then led to dendritic outgrowth and up-regulation of glutamatergic synaptic transmission in rat cerebral cortical neurons [20]. These observations indicate that CD47 and SIRPα, which are differentially expressed on dendrites and axons, could generate a directional intercellular communication system that contributes to the formation and/or regulation of neural networks [7].

In a previous study, we also assessed the behavioral significance of CD47 and SIRPα, and revealed that these molecules are involved in the regulation of immobility in the Porsolt forced swim test in mice [21]. In particular, both mice expressing a form of SIRPα that lacks most of the cytoplasmic region (SIRPα mutant mice) and CD47 knockout (KO) mice exhibited prolonged immobility in the forced swim test, suggesting that depression-like behavior, as assessed by this test, is increased in the mice; however, in SIRPα mutant mice, no significant effects were detected in the tail suspension test [21]. It was determined that phosphorylation of the cytoplasmic region of SIRPα, which requires binding of CD47 to SIRPα, was induced by forced swim stress, but not tail suspension stress (Table S1) [21]. These findings indicate that the CD47-SIRPα signal regulates depression-like behavior in the response to stress that leads to phosphorylation of SIRPα [21]. It was also previously reported that CD47 mRNA levels are significantly higher in rats showing good retention performance in an inhibitory avoidance learning paradigm than in rats exhibiting poor retention performance [22], and that memory retention of CD47 KO mice is significantly impaired in an inhibitory avoidance learning paradigm [23] (Table S1). Those observations suggest that CD47 may be involved in the regulation of fear memory in rodents [22,23]. However, other aspects of CD47's effects on behavior remain largely unknown.

The objective of the present study was to further investigate the behavioral phenotypes of CD47 KO mice by subjecting the

mutants and their wild-type littermates to a comprehensive behavioral test battery. The test battery included wire hang, grip strength, rotarod, hot plate, gait analysis, Crawley's three-chamber social approach, social interaction (home cage/novel environment), open field, startle response/prepulse inhibition (PPI), light/dark transition, elevated plus maze, tail suspension, fear conditioning, and Barnes maze tests. A series of tests revealed novel phenotypes of CD47 KO mice including a decreased PPI and abnormal social interaction.

Results

1. General Health, Motor Function, and Nociception in CD47 KO Mice

There were no significant differences between CD47 KO mice and their wild-type littermates in body weight (Figure 1A; $F_{1,38} = 0.309$, $p = 0.5814$) or body temperature (Figure 1B; $F_{1,38} = 1.216$, $p = 0.2771$). Measures of neuromuscular strength and motor coordination learning likewise did not differ between the genotypes. Specifically, grip strength (Figure 1C; $F_{1,38} = 0.029$, $p = 0.8662$), latency to fall in the wire hang test (Figure 1D; $F_{1,38} = 0.005$, $p = 0.9462$), and latency to fall off the rotarod (Figure 1E; $F_{1,38} = 1.429$, $p = 0.2393$) did not differ significantly between CD47 KO and wild-type mice. There was also no significant difference in nociception between CD47 KO and wild-type mice as measured by the first paw response the hot plate test (Figure 1F; $F_{1,38} = 0.466$, $p = 0.4992$). In addition, brain weight did not significantly differ between genotypes (wild-type mice, 0.478 ± 0.005 g, n = 14; CD47 KO mice, 0.488 ± 0.004 g, n = 12; Student's *t*-test, p = 0.1338).

The gait pattern of CD47 KO mice was also examined. CD47 KO mice showed significant reductions in stance width for both front and hind paws compared to wild-type mice (front paws, $F_{1,37} = 8.410$, $p = 0.0062$, Figure 1G; hind paws, $F_{1,37} = 21.075$, $p < 0.0001$, Figure 1G). In addition, there was a significant difference in paw angles for hind paws (Figure 1H; $F_{1,37} = 5.462$, $p = 0.0250$) but not for front paws between the genotypes (Figure 1H; $F_{1,37} = 1.633$, $p = 0.2093$). Specifically, the stance widths of front and hind paws in CD47 KO mice were narrower than those of wild-type mice, possibly reflecting improved postural adjustments for stability, similar to those previously demonstrated during recovery from injury after a locomotor training paradigm [24]. Paw placement angles for the hind paws were also narrower in CD47 KO mice than in wild-type mice. It is known that more open angles of the hind paws are associated with ataxia, spinal cord injury, and demyelinating disease [25]. These findings suggest that CD47 is involved in the regulation of gait in mice and that deficiency of CD47 may in fact lead to improved motor coordination.

2. Decreased Prepulse Inhibition (PPI) in CD47 KO Mice

To assess whether deficiency of CD47 affects sensorimotor gating in mice, CD47 KO mice were subjected to startle response/PPI tests. CD47 KO mice displayed normal acoustic startle responses to the 110 dB and 120 dB startle stimuli (Figure 2A; genotype effect, $F_{1,38} = 1.209$, $p = 0.2785$, two-way repeated measures ANOVA) but reductions in PPI compared to wild-type mice (Figure 2B; genotype effect, $F_{1,38} = 18.868$, $p = 0.0159$, two-way repeated measures ANOVA). PPI in the mutants was significantly lower than that of wild-type mice when the startle stimulus was 120 dB (Figure 2B; genotype effect, $F_{1,38} = 4.304$, $p = 0.0448$, two-way repeated measures ANOVA) and tended to be lower when the startle stimulus was 110 dB (Figure 2B; genotype effect, $F_{1,38} = 3.984$, $p = 0.0531$, two-way repeated measures ANOVA). These results suggest impaired sensorimotor gating in CD47 KO mice.

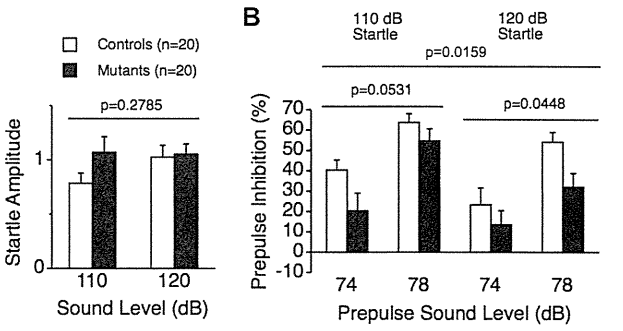

Figure 2. Normal startle response and decreased PPI in CD47 KO mice. (A) CD47 KO mice demonstrated normal acoustic startle responses to the 110 dB and 120 dB startle stimuli. (B) CD47 KO mice showed a significant reduction in PPI for the 74 and 78 dB prepulse sound level compared to wild-type mice. PPI in the mutants was significantly lower than that in wild-type mice when the startle stimulus was 120 dB, whereas only a trend for reduced PPI was observed in the mutants when startle stimulus was 110 dB. CD47 KO mice, n = 20; wild-type mice, n = 20.
doi:10.1371/journal.pone.0089584.g002

3. Abnormal Social Behaviors in CD47 KO Mice

CD47 KO mice were also subjected to Crawley's three-chamber social approach test. This test allows for both a sociability and a social novelty preference test. Importantly, the sociability assay assesses social behavior independently of differences in locomotor activity because the social preference of mice can be quantified by comparing the time spent around a wire cage containing a stranger mouse versus the time spent around an empty cage [26]. In the sociability test, there was no significant genotype effect on ratio of time spent around cage with stranger to total time spent with both cages (Mann-Whitney U-test, $p = 0.4819$). Next, we compared time spent around cage with stranger and that of empty cage within each genotype. There were no significant differences between time spent around the cage with stranger 1 and time spent around the empty cage in the mutants (Figure 3A; $t_{19} = 1.364$, $p = 0.1884$), while in wild-type mice, time spent around the cage with stranger 1 was significantly longer than time spent around the empty one (Figure 3A; $t_{19} = 3.584$, $p = 0.0200$). Moreover, CD47 KO mice showed no significant differences in time spent among the three chambers (Figure 3B, D; stranger 1 side versus empty cage side, $t_{19} = 0.353$ $p = 0.7280$; stranger 1 side versus center, $t_{19} = 1.650$, $p = 0.1154$; center side versus empty cage side, $t_{19} = -1.150$, $p = 0.2643$). On the other hand, wild-type mice spent less time in the center chamber than in the other two chambers (Figure 3B, D; stranger side versus empty side, $t_{19} = 0.475$, $p = 0.6404$; center versus stranger side, $t_{19} = 3.584$, $p = 0.0020$; center versus empty side, $t_{19} = -3.268$, $p = 0.0040$). Ratio of time spent in stranger side to center area for CD47 KO mice was significantly smaller than that for wild type mice (Mann-Whitney U-test, $p = 0.0041$). In the sociability test, CD47 KO mice also showed small but significantly greater values for total distance traveled compared to that of their wild-type littermate controls (Figure 3C; $F_{1,38} = 4.319$, $p = 0.0445$). Next, the social novelty preference test was performed. In the social novelty preference test, social behavior was evaluated by contact with the first, already-investigated mouse (stranger 1/familiar side) and a novel mouse (stranger 2/stranger side) in the wire cage. There were no significant differences in time spent around the cage with